Cell Reports
Medicine

Article

Integrative Tumor and Immune Cell Multi-omic Analyses Predict Response to Immune Checkpoint Blockade in Melanoma

Graphical Abstract

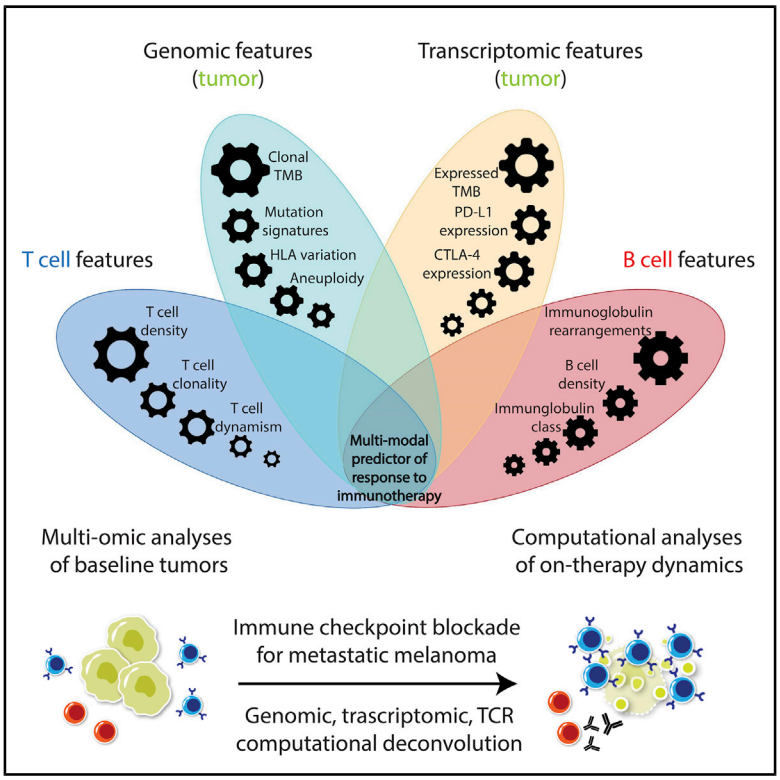

Highlights

- Unmet need for integrated molecular models that interpret immunotherapy response
- Genomic, transcriptomic, and T and B cell sequence data integration by machine learning
- T cell dynamism is a hallmark of response to immune checkpoint blockade
- The combined contributions of B, T, and tumor cell features predict clinical outcome

Authors

Valsamo Anagnostou, Daniel C. Bruhm, Noushin Niknafs, ..., Drew M. Pardoll, Suzanne L. Topalian, Victor E. Velculescu

Correspondence

stopali1@jhmi.edu (S.L.T.), velculescu@jhmi.edu (V.E.V.)

In Brief

Anagnostou et al. integrate genomic, expression, and immune cell repertoire analyses to gain insights into the crosstalk between cancer and immune cells during immunotherapy for melanoma. These findings suggest that the complex phenotype of tumor immune infiltrates combined with genomic features of tumor cells are relevant for determining clinical outcomes.

Anagnostou et al., 2020, Cell Reports Medicine *1*, 100139
November 17, 2020
https://doi.org/10.1016/j.xcrm.2020.100139

CellPress

Cell Reports Medicine

CellPress
OPEN ACCESS

Article

Integrative Tumor and Immune Cell Multi-omic Analyses Predict Response to Immune Checkpoint Blockade in Melanoma

Valsamo Anagnostou,[1,2,9] Daniel C. Bruhm,[1,9] Noushin Niknafs,[1] James R. White,[1] Xiaoshan M. Shao,[1] John William Sidhom,[1,2] Julie Stein,[2,3] Hua-Ling Tsai,[1] Hao Wang,[1] Zineb Belcaid,[1,2] Joseph Murray,[1,2] Archana Balan,[1] Leonardo Ferreira,[1] Petra Ross-Macdonald,[4] Megan Wind-Rotolo,[4] Alexander S. Baras,[2,3] Janis Taube,[2,3] Rachel Karchin,[1] Robert B. Scharpf,[1] Catherine Grasso,[5,6] Antoni Ribas,[5,7] Drew M. Pardoll,[1,2] Suzanne L. Topalian,[1,2,8,*] and Victor E. Velculescu[1,2,3,10,*]

[1]The Sidney Kimmel Comprehensive Cancer Center, Johns Hopkins University School of Medicine, Baltimore, MD 21287, USA
[2]The Bloomberg-Kimmel Institute for Cancer Immunotherapy, Johns Hopkins University School of Medicine, Baltimore, MD 21287, USA
[3]Department of Pathology, Johns Hopkins University School of Medicine, Baltimore, MD 21287, USA
[4]Bristol-Myers Squibb, Princeton, NJ 08540, USA
[5]Jonsson Comprehensive Cancer Center at the University of California, Los Angeles (UCLA), Los Angeles, CA, USA
[6]Cedars-Sinai Medical Center, Los Angeles, CA, USA
[7]Parker Institute for Cancer Immunotherapy, San Francisco, CA, USA
[8]Department of Surgery, Johns Hopkins University School of Medicine, Baltimore, MD 21287, USA
[9]These authors contributed equally
[10]Lead Contact
*Correspondence: stopali1@jhmi.edu (S.L.T.), velculescu@jhmi.edu (V.E.V.)
https://doi.org/10.1016/j.xcrm.2020.100139

SUMMARY

In this study, we incorporate analyses of genome-wide sequence and structural alterations with pre- and on-therapy transcriptomic and T cell repertoire features in immunotherapy-naive melanoma patients treated with immune checkpoint blockade. Although tumor mutation burden is associated with improved treatment response, the mutation frequency in expressed genes is superior in predicting outcome. Increased T cell density in baseline tumors and dynamic changes in regression or expansion of the T cell repertoire during therapy distinguish responders from non-responders. Transcriptome analyses reveal an increased abundance of B cell subsets in tumors from responders and patterns of molecular response related to expressed mutation elimination or retention that reflect clinical outcome. High-dimensional genomic, transcriptomic, and immune repertoire data were integrated into a multi-modal predictor of response. These findings identify genomic and transcriptomic characteristics of tumors and immune cells that predict response to immune checkpoint blockade and highlight the importance of pre-existing T and B cell immunity in therapeutic outcomes.

INTRODUCTION

Cutaneous melanoma, often induced by the carcinogen ultraviolet (UV) radiation, bears a high tumor mutation burden (TMB), and advanced metastatic disease responds to first-line anti-PD-1 therapy administered alone or combined with anti-CTLA-4 at rates of 44% and 58%, respectively.[1,2] A higher mutation and neoantigen load[3–6] and a lower degree of tumor aneuploidy[7] have been linked with clinical benefit from immune checkpoint blockade for patients with melanoma. Tumor-intrinsic features, such as JAK1/JAK2 mutations,[8] PTEN loss,[9] neoantigen loss,[10] antigen presentation deficiency,[11] WNT/β-catenin signaling,[12,13] and interferon-γ signaling,[14] affect the recruitment and activation of T cells to the tumor microenvironment and may therefore mold the anti-tumor immune response. In addition to intrinsic tumor characteristics, the composition of the tumor microenvironment has been shown to influence response and resistance to immune checkpoint blockade.[15] T cell states determined by deconvolution of bulk RNA sequencing data[16] or single-cell approaches[17] have been linked to anti-tumor immunity, underlying the multifaceted mechanisms of therapeutic response and resistance.

The complex crosstalk between tumor and immune cells during immune checkpoint blockade highlights the unmet need for development of integrated models for interpreting anti-tumor immune responses and predicting clinical outcome. Emerging data on nuanced genomic features[18–20] and the variable quality of the anti-tumor immune response in the setting of immunotherapy[21] highlight this clinical need for developing molecular platforms that capture the complexities of the cancer-immune system crosstalk. Furthermore, although pre-existing and on-treatment T cell infiltration has been shown to associate with response to immune checkpoint blockade in melanoma,[15,21] data are only beginning to emerge on the potential contribution of B cell

subsets to anti-tumor immune responses.[22–25] Intratumoral B cell infiltration, especially in the context of tertiary lymphoid structures, has been associated with improved response to immune checkpoint blockade in metastatic melanoma.[24,25] In this study, we have combined comprehensive genomic, transcriptomic, and immune cell repertoire analyses to gain insight into the dynamic interplay between cancer and immune cells during immune checkpoint blockade in melanoma.

RESULTS

Overall Approach, Cohort Characteristics, and Response Assessment

We performed comprehensive genomic and transcriptomic tumor analyses in conjunction with T cell repertoire analyses for 64 melanoma patients treated with immune checkpoint blockade as part of the CheckMate-038 clinical trial (NCT01621490; Figure S1; Table S1A). The purpose of Checkmate-038 was to investigate the mechanism of action of nivolumab and nivolumab in combination with ipilimumab, including its ability to modulate immune function and to overcome tumor escape, in subjects with advanced melanoma. Objective response was defined as complete or partial response based on RECIST 1.1 radiographic assessments. To explore the genomic landscape of these tumors, we performed whole-exome sequencing (WES) of matched tumor-normal pairs and utilized transcriptome analyses (RNA sequencing [RNA-seq]) and T cell receptor (TCR) sequencing (TCR-seq) to assess baseline and on-treatment immune repertoire composition (STAR Methods; Figure S1). The clinical outcomes of radiographic best overall response (BOR) by radiology review, progression-free survival (PFS), and overall survival (OS) were correlated with WES, TCR-seq, and RNA-seq data.

Genomic Determinants of Clinical Outcome

Tumors from responding patients harbored a higher TMB than those that did not respond to therapy (false discovery rate [FDR]-adjusted p = 0.0048; Table 1); however, there was a substantial overlap in TMB values of baseline tumors among responders and non-responders (Figure 1). Tumors from responders harbored a higher number of mutations independent of the type or functional consequence of sequence alterations (FDR-adjusted p = 0.0048), and these findings were more pronounced in the ipilimumab/nivolumab treatment group (FDR-adjusted p = 0.0013; Table 1). Tumors of responding patients harbored a higher clonal mutation fraction, which was more prominent in the ipilimumab/nivolumab group (FDR-adjusted p = 0.0037 and p = 0.0013 for all patients and patients receiving ipilimumab/nivolumab, respectively). Additionally, major histocompatibility complex (MHC) class I and II mutation-associated neoantigens computationally derived from non-synonymous mutations revealed that MHC class I and MHC class II neoantigen load was significantly higher in tumors from responding patients (Table 1). TMB predicted PFS, but not OS, for both ipilimumab/nivolumab- and nivolumab-treated patients (Figure S2). Consistent with the notion that an increased number of somatic mutations in melanoma are related to UV exposure, we observed that a UV-related mutation signature was more prominent in tumors from responding patients, especially in the ipilimumab/nivolumab group (FDR-adjusted p = 0.03 and p = 0.0096, respectively; Table 1). As only expressed neoantigens could potentially be presented and induce the priming and activation of neoantigen-specific T cells, we evaluated the expression of transcripts containing single base substitutions that we had identified through whole-exome analyses (Tables S1B and S1C). Interestingly, whole-exome sequence data combined with transcriptome data revealed that the mutation frequency in expressed genes (expressed mutation burden) more accurately predicted OS than TMB alone (Figure S2).

We subsequently sought to identify genomic alterations in driver genes and pathways that may be selectively associated with therapeutic response or resistance after adjusting for TMB (Tables S1B and S1D). We did not identify any differences in sequence alterations in driver genes among tumors from responding versus non-responding patients (Figure 1). Low-density lipoprotein (LDL)-receptor-related protein 1B (*LRP1B*) and eyes shut homolog (*EYS*) genes appeared to be differentially mutated in responders; however, these genes span 13,891 bp and 9,653 bp, respectively, and therefore, the higher frequency of sequence alterations observed is most likely a reflection of the expected number of passenger mutations in these genes rather than driver events (Table S1D). There was a non-significant trend in enrichment of *ERBB4* and *ANK3* mutations in tumors of responders, likely reflecting TMB-high tumors (TMB-adjusted p = 0.133 and p = 0.058, respectively; Table S1D). We subsequently assessed enrichment or mutual exclusivity of genomic alterations in oncogenic pathways, including DNA damage repair genes, chromatin-regulating genes, and the Wnt and phosphatidylinositol 3-kinase (PI3K)/AKT/PTEN pathways, but we did not identify differential mutation clustering in responders versus non-responders. As an example, we identified a case of a radiographic responder with disproportionally short overall survival whose tumor harbored biallelic inactivation of PTEN (patient 40002) but also a patient treated with nivolumab monotherapy (patient 30050) who achieved a long progression-free and overall survival (24-month PFS and OS) despite harboring a homozygous deletion in *PTEN* (Figures 1 and S3). These findings suggest that PI3K-AKT pathway activation is not always linked with inferior outcomes to immune checkpoint blockade. We considered the Ras/mitogen-activated protein kinase (MAPK) pathway in particular, given the high frequency of BRAF mutations in cutaneous melanoma as well as the potentially immunosuppressive role of the MAPK pathway;[26] however, no differences were noted when either all mutations or hotspot mutations were considered (Figure S3). Additionally, although a potential association of mutant *BRAF* with improved overall survival in patients receiving combination PD-1 and CTLA-4 blockade compared to anti-PD-1 monotherapy has been reported,[27] we did not identify differential clinical outcomes based on *BRAF* mutation status in our study (Figure 1).These data are consistent with previous findings in melanoma that *BRAF* V600E/K mutations do not predict response to nivolumab monotherapy or ipilimumab/nivolumab combination therapy.[1]

Analyses of copy number changes revealed recurring copy number alterations in a group of genes residing on 11q14.1, and this locus was found to be co-amplified with *CCND1* in a

Table 1. Differential Enrichment Analysis for Genomic, Transcriptomic, and TCR Features for All Patients and Patients in the Ipilimumab/Nivolumab Arm

	All Patients					Patients in the Ipilimumab/Nivolumab Arm				
Feature	NR (Count)	R (Count)	Mean Value (NR)	Mean Value (R)	FDR	NR (Count)	R (Count)	Mean Value (NR)	Mean Value (R)	FDR
Genomic Features										
TMB	20	25	227	694	0.0048	15	21	172	768	0.0013
SBS	20	25	223	684	0.0048	15	21	168	758	0.0013
Indels	20	25	4	10	0.0376	15	21	3	10	0.0125
Non-synonymous	20	25	200	622	0.0048	15	21	151	688	0.0013
Nonsense mutations	20	25	14	37	0.0059	15	21	10	41	0.0026
Splice site mutations	20	25	11	28	0.0133	15	21	8	32	0.0026
Frameshift mutations	20	25	2	6	0.0288	15	21	2	6	0.0096
Clonal mutations	18	24	173	666	0.0037	14	20	160	745	0.0013
Clonal mutations (%)	18	24	0.92	0.96	0.0048	14	20	0.92	0.97	0.0054
UV mutation signature (%)	20	25	0.41	0.64	0.0313	15	21	0.35	0.66	0.0096
Candidate MANAs (I)	20	25	146	433	0.0048	15	21	107	479	0.0013
Expressed MANAs (I)	20	25	106	300	0.0057	15	21	78	331	0.0013
Immunogenic MANAs (II)	20	25	4,218	14,700	0.0016	15	21	3,264	16,1734	0.0013
Tumor Aneuploidy Features										
Estimated ploidy	18	24	2.52	2.90	0.1851	14	20	2.60	3.01	0.2249
Allelic imbalance (%)	18	25	0.23	0.17	0.1912	14	21	0.23	0.16	0.3303
CN entropy	18	24	1.41	1.50	0.9012	14	20	1.43	1.55	0.7770
HLA class I alleles	19	25	5	5	0.9012	14	21	5	5	0.7770
TCR Features										
TCR rearrangements	23	25	5,137	8,308	0.0018	15	20	4,939	8,338	0.0089
TCR productive clonality	23	25	0.11	0.15	0.0865	15	20	0.12	0.16	0.0765
Transcriptomic Features										
Expressed SBS	18	23	67	150	0.0124	13	19	53	166	0.0040
Ig rearrangements	18	23	2	7	0.0016	13	19	2	8	0.0016
TIGIT expression (TPM)	18	23	2.35	11.80	0.0007	13	19	1.67	12.47	0.0016
PDL1 expression (TPM)	18	23	3.70	14.16	0.0007	13	19	2.67	15.46	0.0011
LAG3 expression (TPM)	18	23	3.24	15.95	0.0016	13	19	2.54	17.64	0.0016
PD1 expression (TPM)	18	23	1.12	4.24	0.0016	13	19	0.55	4.45	0.0016
LCA expression (TPM)	18	23	24.04	72.60	0.0016	13	19	19.35	79.94	0.0018
CTLA4 expression (TPM)	18	23	4.60	6.56	0.0189	13	19	3.58	7.09	0.0061

Differences in genomic, tumor aneuploidy, transcriptomic, and TCR features were assessed by the Mann-Whitney test, p values were corrected using the Benjamini-Hochberg procedure, and the associated false discovery rate (FDR) values were calculated. Candidate mutation-associated neoantigens with a predicted MHC class I affinity of <500 nM were included in the analyses. Candidate mutation-associated neoantigens with a predicted MHC class II affinity of <500 nM and a differential agretopic index >2 were considered immunogenic (see STAR Methods). Patients in the single-agent nivolumab arm are not shown, as the small sample size (n = 12) precluded firm statistical analyses and comparisons between responders and non-responders for this arm. CN, copy number; FDR, false discovery rate; HLA, human leukocyte antigen; Ig, immunoglobulin; MANA, mutation-associated neoantigen; NR, non-responder; R, responder; SBS, single base substitution; TCR, T cell receptor; TMB, tumor mutation burden; TPM, transcripts per million.

fraction of cases (Figure 1; Table S1E). The *AAMDC*, *CLNS1A*, *INTS4*, *KCTD14*, *NDUFC2*, *NDUFC2-KCTD14*, *RSF1*, and *THRSP* loci were found to be co-amplified in melanomas from five non-responders but in none from responders, with a trend toward significance after FDR correction (Fisher's exact p = 0.013; FDR-adjusted p = 0.094; Figure 1; Table S1D). The locus contains *RSF1*, a chromatin-regulating gene required for nucleosomal assembly, and amplifications of *RSF1* may lead to a more "closed" chromatin state,[28] decreased transcription, and potentially a lower number of expressed mutation-associated neoantigens. We further assessed whether the amplification resulted in increased gene expression and found that the *AAMDC*, *CLNS1A*, *INTS4*, *NDUFC2*, and *RSF1* genes were overexpressed in all five tumors that harbored an amplification (Figure S4). To systematically assess the impact of chromosomal imbalances, we performed genome-wide copy number analyses

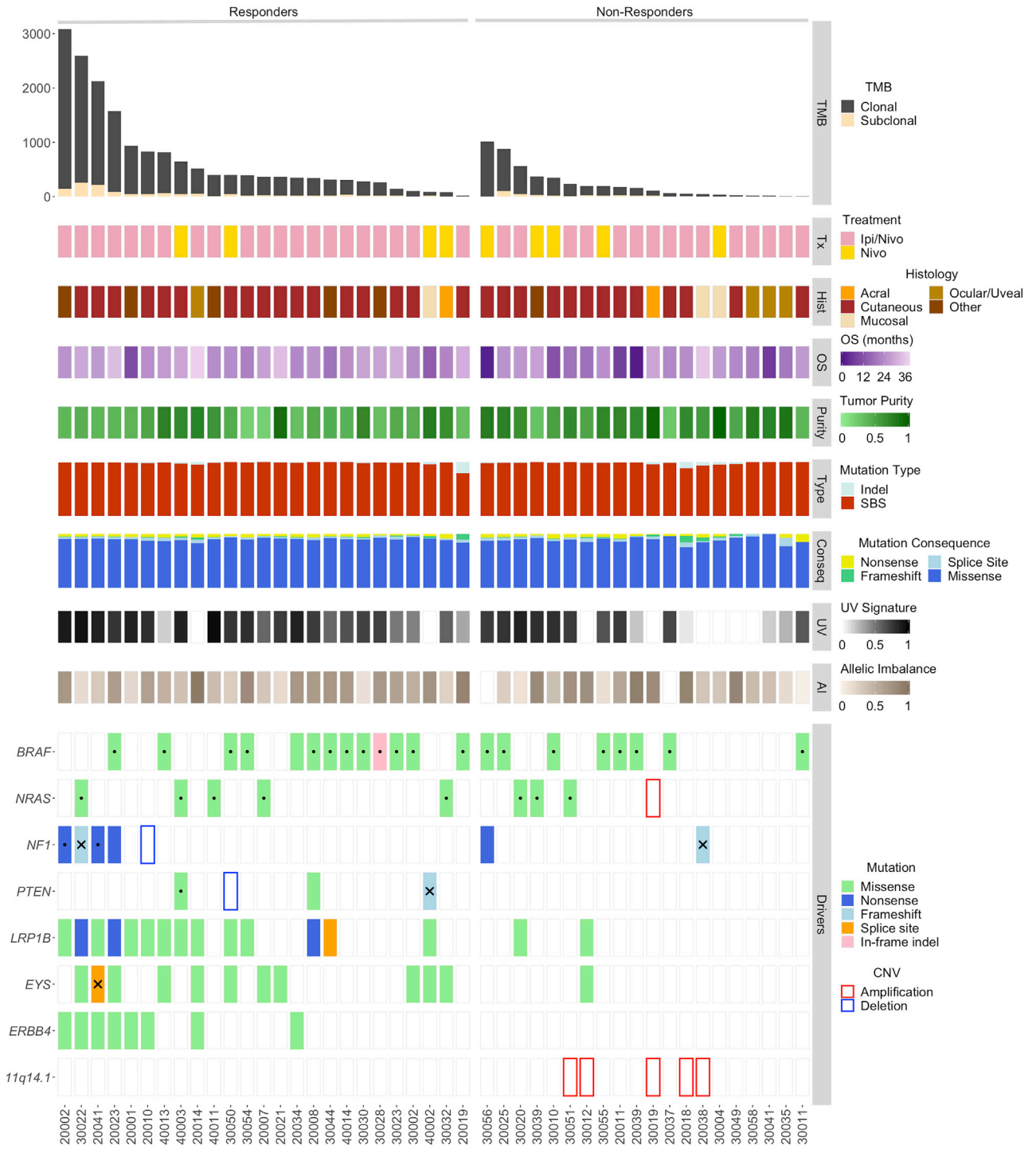

Figure 1. Tumor Genomic Features Associated with Clinical Benefit

Tumors of responding patients had a higher total and clonal TMB compared to non-responders (FDR-adjusted p = 0.0048 and p = 0.0037, respectively). Overall, a higher number of single-base substitutions and indels were found in tumors of responders, which was largely driven by their higher TMB. A UV-related mutational signature was found to be enriched in tumors of responders for all patients and patients in the ipilimumab/nivolumab group (FDR-adjusted p = 0.03 and p = 0.0096, respectively). Following an exome-wide unbiased approach, we investigated potential differential abundance of sequence alterations in tumors of responding patients. *LRP1B* and *EYS* mutations appeared to accumulate in tumors of responding patients (FDR p = 0.058 for both genes and TMB-adjusted p = 0.036 and p = 0.025 for *LRP1B* and *EYS*, respectively), most likely due to the expected larger number of passenger mutations in larger DNA regions. There was a non-significant trend in enrichment of ERBB4 mutations in tumors of responders, likely reflecting TMB-high tumors (TMB-adjusted p = 0.133). There were no

(legend continued on next page)

coupled with tumor purity correction (STAR Methods; Table S1F) and found a trend toward a higher level of aneuploidy in tumors from non-responders (Figure 1). A similar trend was observed in survival analyses such that patients with highly aneuploid tumors had worse PFS and OS, especially in the ipilimumab/nivolumab treatment group (Figure S5). There was no difference in the number of somatic rearrangements as determined by transcriptome analyses between tumors from responding versus non-responding patients (Mann Whitney p = 0.62).

Antigen Presentation Machinery Variation Is Linked with Therapeutic Response

Given the role of antigen presentation diversity in shaping anti-tumor immunity,[29] we analyzed germline and tumor-specific HLA class I and class II genomic variation leveraging whole-exome sequencing from baseline tumors (Table S1G). HLA class I germline zygosity and somatic HLA class I loss of heterozygosity (LOH) events were combined to determine the number of unique HLA class I alleles in tumor cells (Figure 2A). Although HLA class I genetic diversity (germline or somatic) did not appear to correlate with response to immune checkpoint blockade in this cohort, patients with maximal germline heterozygosity for HLA class II had a significantly longer progression-free survival (log rank p = 0.043; Figure 2B). Loss of heterozygosity in HLA class II loci did not appear to correlate with clinical outcome (log rank p = 0.753), suggesting that loss of heterozygosity of the somatic HLA class II loci may not be indicative of an impaired potential to elicit a CD4+ T cell response. Homozygosity at the HLA-DP, and particularly in the HLA-DPB1 locus was associated with significantly longer PFS (log rank p = 0.007 and log rank p = 0.005, respectively; Figures 2C and 2D). The β_2-microglobulin locus frequently underwent monoallelic loss; however, we did not detect an enrichment in concurrent inactivating mutations in tumors from non-responding patients, suggesting that β_2-microglobulin inactivation was an infrequent mechanism of immune evasion in this cohort (Figure 2A). There was a trend toward an anti-correlation between tumor antigen presentation capacity, as determined by the number of distinct HLA class I alleles in the tumor, and TMB (Spearman rho = −0.224, p = 0.14 for all patients and rho = −0.349, p = 0.088 in responders), suggesting that tumors with increased TMB may overcome the evolutionary disadvantage of being more visible to the immune system through HLA loss and diminished neoantigen presentation.[19] Interestingly, a higher expression of all HLA class I and II molecules was noted in baseline tumors from responding patients (Mann-Whitney p = 0.00032 and p = 0.014, respectively), likely reflecting a higher pre-existing lymphocytic intratumoral infiltration of responding tumors (post-leukocyte common antigen [LCA] expression normalization p = 0.29 for HLA-A, B, and C alleles; Figure S6). Similarly, β_2-microglobulin expression was significantly decreased in non-responders independent of biallelic inactivation in the tumor (Mann Whitney p = 0.014), potentially suggesting that the differences in expression are primarily driven by immune cell content in the tumor microenvironment rather than cancer cells (Figure 2A).

Baseline T Cell Features and On-Therapy Dynamics Reflect Clinical Response to Immune Checkpoint Blockade

To assess the T cell repertoire in tumors with differential responses to immune checkpoint blockade, we performed TCR sequencing of baseline and on-therapy tumor-infiltrating lymphocytes (see STAR Methods and Table S1H). These analyses revealed a significantly higher number of unique TCR clones at baseline, signifying an increased density of pre-existing T cells in tumors from responders (FDR p = 0.0018 and p = 0.009 for all patients and patients in the ipilimumab/nivolumab treatment group, respectively; Tables 1 and S1I; Figure 3A). A trend toward a more clonal TCR repertoire was noted in tumors of responding patients (FDR p = 0.09 for all patients and p = 0.08 for the ipilimumab/nivolumab group; Table 1). Patients with highly infiltrated tumors, denoted by a high number of productive TCR rearrangements, had a significantly longer PFS (log rank p = 0.007 and p = 0.005 for all patients and patients in the ipilimumab/nivolumab group, respectively; Figure S5). Baseline intratumoral TCR clonotypic density was associated with relative abundance of T cell transcriptional profiles, consistent with both CD8+ (Spearman rho = 0.606; FDR p = 0.0014) and memory CD4+ (Spearman rho = 0.67; FDR p = 0.0001) phenotypes independent of response to therapy (Tables S1J and S1K).

Importantly, in the on-treatment tumors from responding patients, there was evidence of T cell repertoire changes toward higher clonality (FDR p = 0.02 for all patients and p = 0.015 for patients in the ipilimumab/nivolumab group; Table S1I). Paired analyses of TCR sequencing of baseline and on-treatment tumors from individual patients revealed that clonotypic dynamism (expansions and regressions of TCR clones) were a hallmark of responding patients (Figure 3B). Of note, the fraction of expanding TCR clones significantly correlated with the relative abundance of CD8+ T cells derived from expression data (Spearman rho = 0.52; FDR p = 0.04). These dynamic shifts in the T cell repertoire were reflective of clinical outcome (Figures 3B–3D) such that the fraction of expanding and regressing TCR clones was significantly higher in responders compared to non-responders (FDR p = 0.02 for all patients and p = 0.04 for patients in the ipilimumab/nivolumab group; Table S1I). As CD8+ T cells are functionally rewired to exhausted T cells in an immunosuppressive tumor microenvironment and can be reinvigorated by immune checkpoint blockade,[30,31] we investigated whether a T cell exhaustion transcriptional program was

differences in the abundance of BRAF and NF1 mutations between tumors of responders and non-responders. The *AAMDC*, *CLNS1A*, *INTS4*, *KCTD14*, *NDUFC2*, *NDUFC2-KCTD14*, *RSF1*, and *THRSP* loci on chromosome 11q14.1 were found to be co-amplified in five tumors of non-responders (FDR-adjusted p = 0.094). Genome-wide copy number analyses revealed a trend toward increased tumor aneuploidy in tumors of non-responding patients (denoted by fraction of the genome with complete allelic imbalance; FDR-adjusted p = 0.19). AI, allelic imbalance; BOR, best overall response; CNV, copy number variation; Conseq, mutation consequence; CR, complete response; OS, overall survival; PD, disease progression; PR, partial response; SBS, single-base substitution; SD, stable disease. Dots represent hotspot mutations, and X denotes monoallelic loss of the wild-type allele.

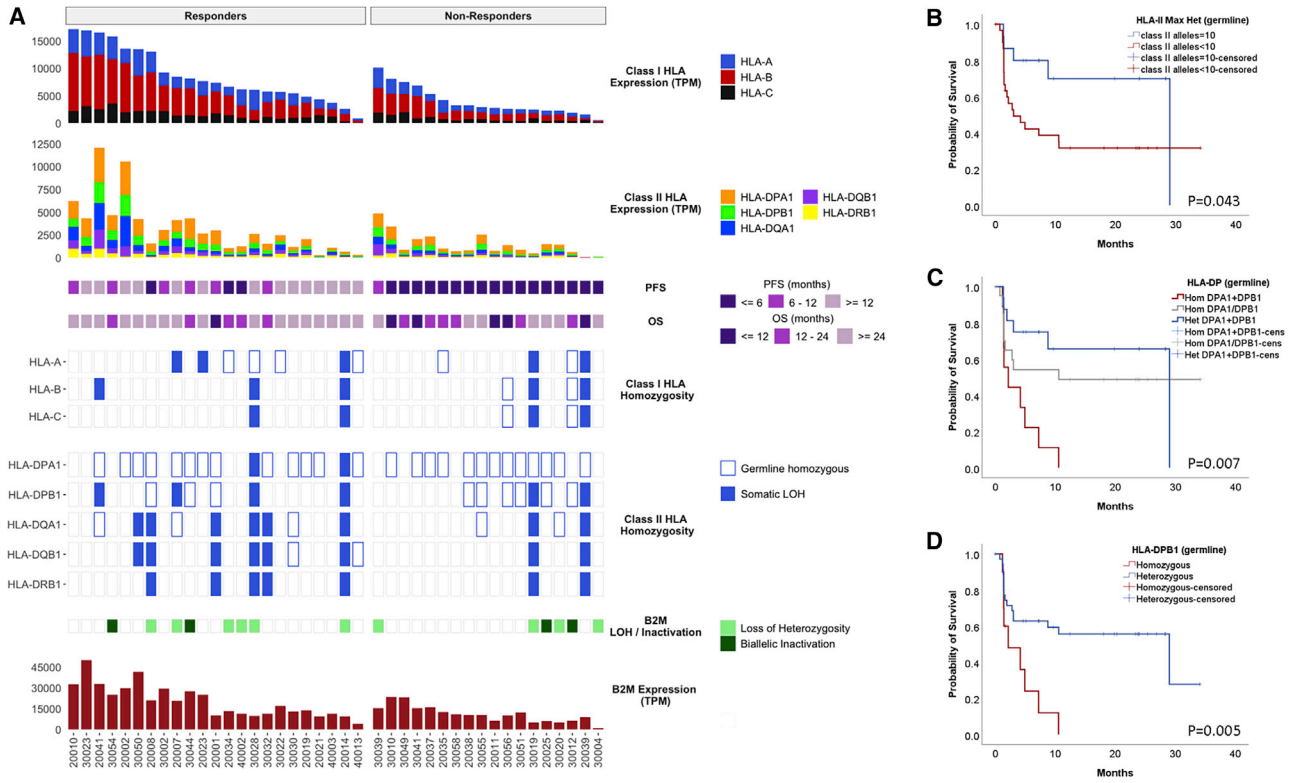

Figure 2. Antigen Presentation Genomic Diversity and Expression Is Associated with Response to Immune Checkpoint Blockade

(A) There were no differences in the number of germline HLA class I alleles or the degree in homozygosity found between responders and non-responders. HLA class I germline zygosity and somatic HLA class I LOH were combined to calculate the unique number of HLA class I alleles in tumor cells. The β_2-microglobulin locus frequently underwent monoallelic loss, but there was no evidence pointing to an enrichment in concurrent inactivating mutations in tumors from non-responder patients. HLA class I and II as well as β_2-microglobulin expression was significantly higher in tumors from responding patients.

(B) HLA class II genotypes for DPA1, DPB1, DQA1, DQB1, and DRB1 were derived from whole-exome sequence data. Patients with maximal heterozygosity for HLA class II (HLA class II alleles = 10) had a significantly longer progression-free survival (log rank p = 0.043).

(C and D) Patients heterozygous at the HLA-PD locus and more specifically at the HLA-DPB1 locus had a significantly longer progression-free survival (log rank p = 0.007 and p = 0.005, respectively).

prominent in baseline tumors of responding patients. Interestingly, we found a significant difference in expression of the high-mobility group (HMG)-box transcription factor TOX between responding and non-responding tumors (Mann Whitney p = 0.0007; Figure S7). This finding supports the notion that CD8+ T cell exhaustion, identified here through TOX expression, may be reversible and result in a therapeutic effect for immune checkpoint blockade.

Differential B Cell Infiltration Is Linked to Therapeutic Response to Immune Checkpoint Blockade in Melanoma

Although T cell activation and their epigenetic/functional state has been shown to be essential for controlling anti-tumor immune responses,[31] there is limited evidence to date for a role of tumor-associated B cells.[22–25] Through analyses of gene fusions using transcriptome data, we identified a higher number of rearrangements involving the immunoglobulin genes in baseline tumors from responders compared to non-responders (FDR-adjusted p = 0.0016; Figure 4A; Tables 1 and S1L), suggesting a greater and potentially more diverse infiltration of B cells. To further investigate this finding, we examined the relative abundance of transcripts from RNA-seq analyses to computationally characterize the extent of immune cell infiltration and infiltrate composition of baseline tumors.[32] Consistent with the rearrangement analysis, we found an enrichment in tumor-associated B cells in baseline tumors of patients with a clinical response (Figures 4B–4E), suggesting that pre-existing B cell infiltration correlates with therapeutic response. Interestingly, the relative abundance of both naive B cells and plasma cells at baseline were significantly higher in responders (Figures 4B, 4D, and 4E) and correlated with the number of productive TCR clonotypes (Spearman rho = 0.472; FDR p = 0.04; Table S1J), suggesting the possibility that these immune cell subsets may interact to generate an effective immune response in the setting of immune checkpoint blockade. There was no correlation between transcriptomic B cell signatures and anatomic location of the tumor analyzed, and we did not observe a higher B cell abundance in lymph node metastasis specimens (Mann Whitney p = 0.2). In addition, we investigated whether the transcriptome-derived B cell enrichment correlated with the approximate density of plasma cells by morphologic assessment in hematoxylin/eosin-stained tissue sections; however, this correlation did not

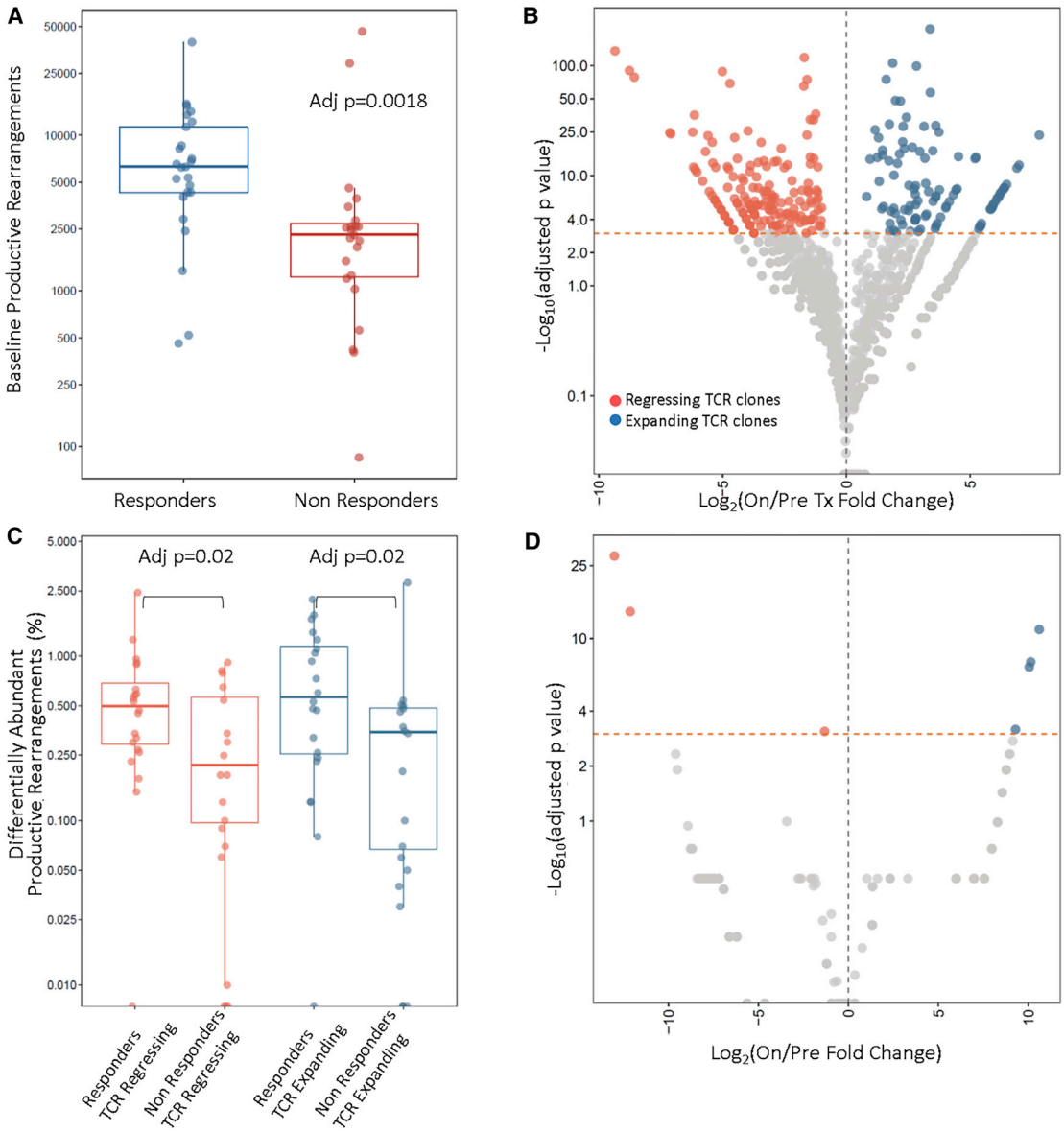

Figure 3. T Cell Receptor Repertoire Features and Dynamics during Immune Checkpoint Blockade Differentiate Tumors of Responders from Non-responders

(A) Differential abundance analysis employing the number of TCR clones revealed an enrichment of unique TCR rearrangements in tumors of responding patients (FDR-adjusted p = 0.0018).

(B) Dynamic shifts in the TCR repertoire composition on therapy were reflective of clinical outcome, such that tumors of responders harbored a higher fraction of expanding and regressing clones. A representative example of TCR repertoire reshaping is shown in (B) for patient 20002, who achieved a complete response on ipilimumab and nivolumab.

(C) Overall, the fraction of expanding and regressing TCR clones was significantly higher in responders compared to non-responders (FDR p = 0.02 for both fractions of responding and regressing clones).

(D) Representative example of TCR repertoire dynamics for a patient experiencing disease progression on the ipilimumab/nivolumab arm; a less dynamic repertoire is observed, denoted by a significantly lower number of clonotypic expansions and regressions after therapy initiation.

reach statistical significance, likely due to the small number of cases in the subset of tumors available for this analysis (n = 26; data not shown).

High pre-existing intratumoral memory B cell abundance correlated with a more-diverse TCR repertoire (Spearman rho = −0.357; p = 0.024; FDR p = 0.2), whereas plasma cell relative abundance was associated with greater degree of T cell infiltration (Spearman rho = 0.367; p = 0.02; FDR p = 0.17) and a more restricted repertoire (Spearman rho = 0.375; p = 0.017; FDR p = 0.15; Table S1J). Unsupervised clustering applied to

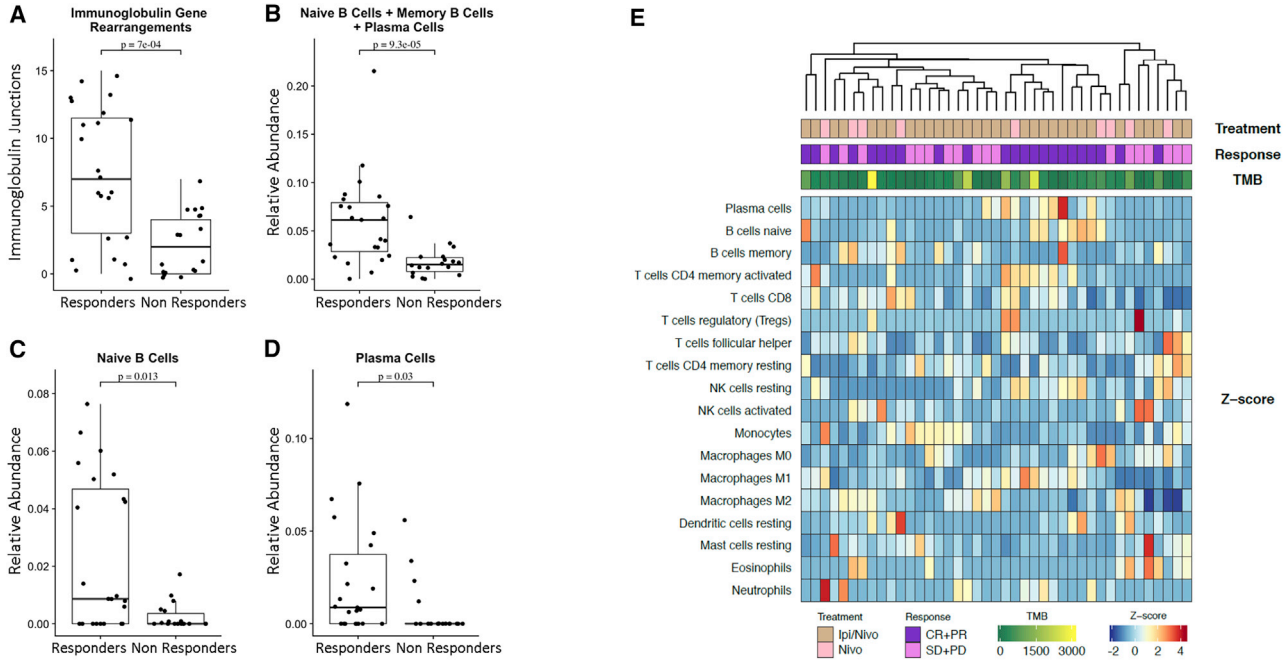

Figure 4. Transcriptome Deconvolution Reveals B Cell Enrichment in Tumors of Responding Patients

(A) Fusion analysis utilizing transcriptome data revealed an enrichment in immunoglobulin rearrangements in tumors of responding patients, which was reflective of a higher pre-existing intratumoral B cell infiltration (Mann Whitney p = 7e−04).

(B) Through gene expression signature analysis and deconvolution of RNA sequence data, we identified an enrichment in tumor associated B cells in baseline tumors of responding patients (Mann Whitney p = 9.3e−05).

(C and D) This observation was driven by enrichment in the naive B cell and plasma cell populations (Mann Whitney p = 0.013 and p = 0.03, respectively).

(E) Through unsupervised clustering of relative abundance of 22 immune-cell-type populations, patients with clinical response to therapy clustered together and showed higher relative abundance in B cell subsets as well as CD8+ T cells. *Z* scores were computed across samples for each immune cell type separately using the relative abundance measurements obtained from CIBERSORT.

the relative abundance of immune cell subsets based on deconvolution of transcriptomic data revealed a cluster of responding tumors with enrichment in B cell subsets (Figure 4E). Patients with tumors harboring a high number of immunoglobulin gene rearrangements had a significantly longer PFS (log rank p = 0.0014 and p = 0.003 for all patients and patients in the ipilimumab/nivolumab group, respectively; Figure S7). Concurrent elevated pre-existing T and B cell infiltration defined tumors from responding patients independent of tumor mutation burden (Figure 5). Characterization of the intratumoral B cell repertoire is critical for understanding B cell immunity. To this end, we assembled B cell immunoglobulin heavy (IgH) and light (IgL) chain CDR3 sequences from bulk RNA-seq data[33] to gain insights into the functional effects of intratumoral B cells in anti-tumor immune responses in the context of immune checkpoint blockade. We identified significantly increased clonal counts for both IgH and IgL chains (Mann Whitney p = 0.00023 and p = 4.69e−05, respectively) in tumors from responding patients, indicating an increased abundance of B cells in tumors from responding patients (Figure S7).

We subsequently evaluated B cell receptor (BCR) clonotypic abundance in baseline tumors, and these analyses were consistent with our previous findings suggesting a higher B cell abundance in tumors from responding patients independent of treatment (FDR-adjusted p = 0.002 and p = 0.002 for all patients and patients in the ipilimumab/nivolumab group; Figure S7; Table S1M). We then investigated the class and subclass composition of the B cell repertoire in baseline tumors and identified an enrichment in IgG1, IgG2, and IgG3 CDR3s in tumors from responding patients (FDR-adjusted p = 0.001, p = 0.02, and p = 0.001, respectively; Table S1M). Importantly, tumors from responding patients showed a trend toward a more clonal BCR repertoire (FDR-adjusted p = 0.076; Figure S7; Table S1M). Immunoglobulin class and subclass differential abundance analysis revealed a higher abundance of IgG1, IgG2, and IgG3 CDR3s in on-treatment tumors (FDR-adjusted p = 0.002, p = 0.008, and p = 0.003; Table S1M). BCR clonal dynamics, by means of significant expansions and regressions, were more evident for IgG3 CDR3s (FDR p = 0.067 and p = 0.047 for clones increasing and decreasing in frequency, respectively). Our findings suggest unique functional states of B cells in tumors from patients with differential responses to immune checkpoint blockade and further highlight that the complex phenotype of the immune infiltrate, beyond T cell infiltration, is relevant for determining clinical outcome.

Tumor Cell Evolutionary Trajectories during Immune Checkpoint Blockade

We subsequently modeled temporal tumor dynamics, employing an approach that combined exome with pre- and on-treatment

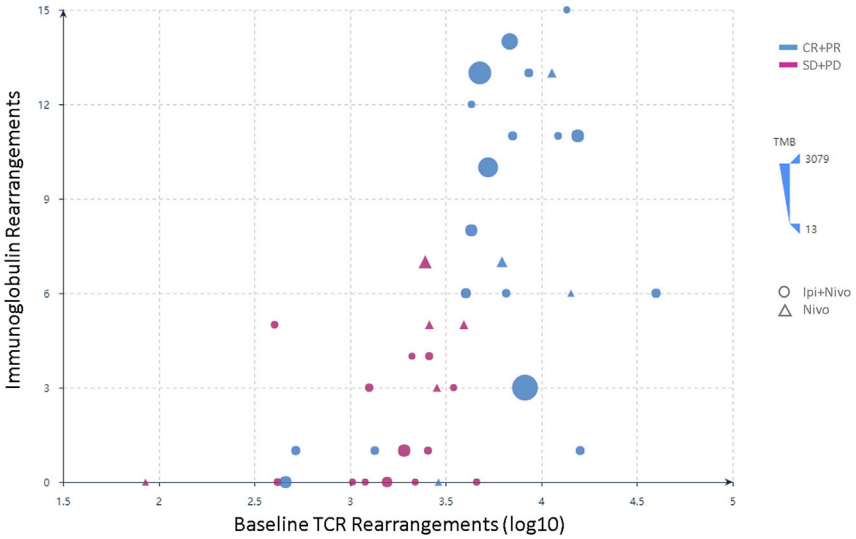

Figure 5. B and T Cell Interactions Shape Clinical Responses to Immune Checkpoint Blockade Independent of Tumor Mutation Burden

Immunoglobulin rearrangements highly correlated with TCR rearrangements in tumors of responders (Spearman rho = 0.68; p = 1e−06), delineating a group of patients that derived benefit from immune checkpoint blockade (shown as blue circles and triangles and clustered in the right upper corner of the plot). This correlation between pre-existing B and T cell rearrangements with each other and with response to therapy was not affected by TMB. Circles indicate treatment with ipilimumab and nivolumab, although triangles denote treatment with nivolumab. Responders are shown in blue and non-responders in magenta. The size of each point (solid circle or triangle) is proportional to the TMB of the corresponding baseline tumor.

transcriptome data (STAR Methods). A Bayesian generalized linear mixed effects model was utilized to account for changes in tumor purity between the pre- and on-therapy tumors and capture molecular response patterns for patients with differential clinical responses to immune checkpoint blockade. We tracked changes in frequencies of expressed single-base substitutions and mapped temporal trajectories of tumor cells to clinical outcomes. Overall, analyses of tumors from responding patients revealed contractions of the expressed mutation repertoire, in biopsies obtained 2–4 weeks after treatment initiation. In contrast, tumors of non-responders were predominated by retention of expressed mutations signifying a pattern of molecular primary resistance that predicted clinical disease progression (Figure S8). Of note, tumors of responding patients 30028, 20021, 30032, 30023, and 30050 showed a pattern of expressed mutation retention, likely attributed to the timing of the on-treatment tumor biopsy that preceded tumor clearance. Patient 30020 showed a clear pattern of molecular response that was reflected in a long overall survival of 26.1 months, but not captured by early radiographic assessments denoting disease progression at 1.4 months. Conversely, the tumor of non-responding patient 20001 showed a molecular progression pattern that was reflective of eventual clinical outcome (OS of 10.2 months), despite a radiographic response assessment of partial response. These findings suggest that molecular responses reflect tumor cell dynamics during therapy and may provide early predictors of long-term clinical outcome.

Integrative Modeling Incorporating Genomic, Transcriptomic, and Immune Characteristics

The complexity of tumor and immune cell interactions during immune checkpoint blockade suggests that integrative approaches may identify more nuanced biomarkers of therapeutic response. We first assessed correlations among baseline genomic, transcriptomic, and T cell repertoire features and identified clusters of interrelated variables (Figure 6A). We applied random forests, an ensemble tree method, to integrate these features into a multi-modal predictor of therapeutic response and analyzed the utility of our approach in predicting clinical response. The model incorporated training and testing with a 10-fold cross-validation approach, and feature selection, including elimination of collinear features, was embedded in the cross-validation (STAR Methods). Our approach demonstrated a high prediction accuracy with an area under the curve (AUC) of 0.866 (95% confidence interval [CI]: 0.738–0.994; Figure 6B). The integrated classifier outperformed TMB (AUC = 0.583; 95% CI: 0.377–0.79) and PD-L1 expression (AUC = 0.726; 95% CI: 0.552–0.9; Figure S9). We subsequently employed multivariable Cox proportional hazards regression analysis to evaluate the combined contribution of B cell, T cell, and tumor features in predicting outcome. The combined contribution of immunoglobulin rearrangements, TCR productive clones, PD-L1 expression, and expressed mutation burden was utilized to compute a risk score and classify patients in high- and low-risk groups (STAR Methods). Patients classified in the high-risk category had a significantly shorter PFS compared to patients in the low-risk category (median PFS 1.43 months versus 29.01 months; log rank p = 9.07e−05; HR = 5.92; 95% CI: 2.25–15.58; Figure 6C; Table S1N). This was also evident in the ipilimumab/nivolumab group (median PFS 1.43 months versus 29.01 months; log rank p = 7.05e−05; HR = 8.09; 95% CI: 2.53–25.93; Figure 6D).

DISCUSSION

There is an unmet clinical need for development of integrated biomarkers of response to immune checkpoint blockade that reveal the underlying biology of the anti-tumor immune response and predict clinical outcome. In this study, we report multifactorial tumor biopsy analyses in a cohort of melanoma patients receiving immune checkpoint blockade, including genomic and pre- and on-therapy transcriptomic and T cell repertoire characteristics. Our findings highlight the multifaceted interactions between the tumor and the immune system and suggest the importance of pre-existing T and B cell immunity in driving clinical responses to immune checkpoint blockade.

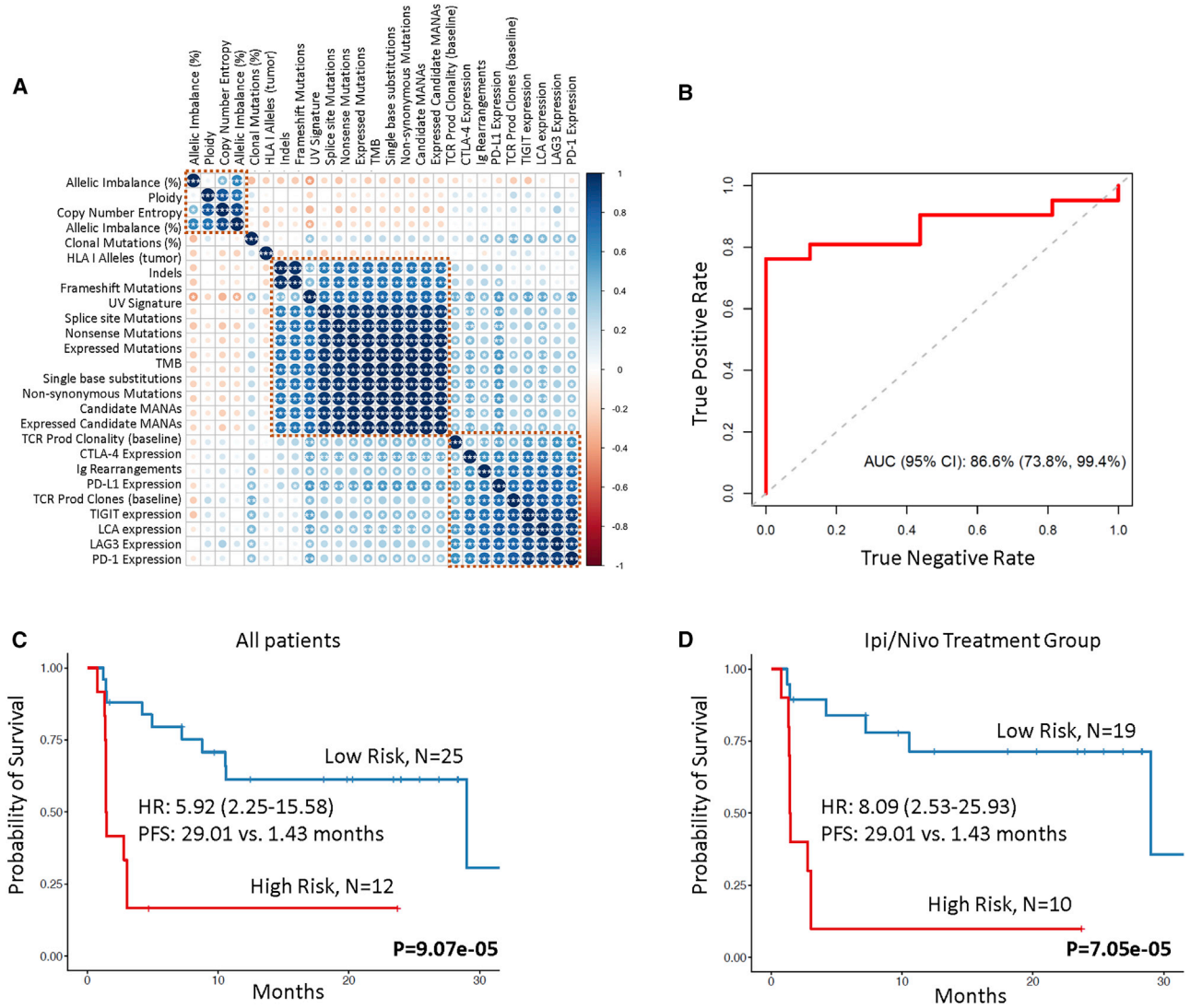

Figure 6. Multi-parameter Integrative Modeling Accurately Predicts Therapeutic Outcome

(A) Non-parametric correlations among genomic, transcriptomic, and T cell repertoire features were assessed by the Spearman's rho statistic, and p values were corrected for multiple comparisons. The color of each dot refers to the Spearman rho coefficient value (darkest blue being 1 and darkest red being −1), and the size of each dot is proportional to the strength of the correlation. ***FDR-adjusted $p < 0.05$, **FDR-adjusted $p < 0.1$, and *FDR-adjusted $p < 0.2$.

(B) Random forests were employed to integrate genomic, transcriptomic, and TCR features following training and testing with 10-fold cross-validation and resulted in an integrated model with an area under the curve of 0.866.

(C) Immunoglobulin rearrangements, TCR productive clones, PD-L1 expression, and expressed mutation load were combined in a multivariable Cox proportional hazards regression model, and a risk score was calculated for each case based on the weighted contribution of each parameter. The second tertile of the risk score was used to classify patients in high-risk (top 33.3%) and low-risk (bottom 66.6%) groups. Patients with a higher risk score had a significantly shorter progression-free survival compared to patients at low risk for disease progression (median PFS 1.43 months versus 29.01 months; log rank p = 9.07e−05; HR = 5.92; 95% CI: 2.25–15.58).

(D) This outcome was also pronounced in the ipilimumab/nivolumab group (median PFS 1.43 months versus 29.01 months for high- and low-risk score patients, respectively; log rank p = 7.05e−05; HR = 8.09; 95% CI: 2.53–25.93).

Multifactorial biomarker models have the potential to be highly predictive of clinical outcomes following immune checkpoint blockade, compared to unidimensional markers.[19,20,34] Several transcriptomic signature-based models have been proposed to predict therapeutic response for patients treated with immune checkpoint blockade,[21,35,36] and the predictive value of gene expression signatures, such as IPRES,[36] TIDE,[35] and IMPRES,[37] was assessed in a recent study utilizing RNA-seq data from a cohort of melanoma patients treated with immune checkpoint blockade.[38] In that study, none of the published immune-predictive signatures accurately predicted clinical response to therapy. We also evaluated the performance of the TIDE algorithm in our

cohort, which generated a receiver operator characteristic (ROC) curve with an AUC of 0.506 (Figure S9). These findings highlight the challenges with gene expression signatures in accurately classifying clinical response to immune checkpoint blockade.

Consistent with the notion that the efficacy of anti-PD-1-based immune checkpoint blockade is based on reinvigoration of the activity of pre-existing anti-tumor effector cells,[15,21] we noted an increased pre-existing T cell infiltration in tumors from responding patients. Importantly, TCR clonotypic expansions and regressions resulted in a more clonal on-therapy TCR repertoire that differentiated responders from non-responders. In line with previous work from our group in non-small cell lung cancer treated with immune checkpoint blockade,[39,40] we noted TCR clonotypic expansions and regressions in the responding tumors that may reflect antigen-driven T cell expansion and antigen-dependent T cell arrest. A companion study utilizing samples from the CheckMate038 clinical trial demonstrated through complementary analyses that T cell infiltration and expression of interferon-ɣ-regulated genes differentiate tumors of responding patients from non-responders to immune checkpoint blockade.[41]

Emphasis has been historically placed on the contribution of cytotoxic CD8+ T cells rather than a combined contribution of T and B cell subsets. B cells modulate T cell responses; however, the functional role of B cells as it relates to clinical benefit to immune checkpoint blockade is incompletely understood. B cell immunity against tumor-associated antigens, in the form of circulating tumor-specific antibodies, has been linked with clinical responses to ipilimumab in the presence of T cell anti-tumor immune responses,[42] but the role of pre-existing B cell immunity in shaping the anti-tumor immune response in the setting of immunotherapy has not been well established.[43] We report a significant enrichment in B cells evidenced by the abundance of immunoglobulin rearrangements as well as by deconvolution of transcriptomic data in tumors from responding patients. Increased immunoglobulin gene rearrangements are a hallmark of antigen-specific B cell responses, potentially consistent, but not confirmed to be tumor-specific in this study. We identified an enrichment in naive B cells in tumors from responding patients; naive B cells play a role in MHC class II antigen presentation[44] and may induce antigen-specific proliferation of naive T cells.[45] The vital contribution of tumor-associated B cells in the anti-tumor immune response is evidenced by depletion of B cells in melanoma patients by anti-CD20 therapy causing a decrease in CD8+ T cell infiltration.[22] Recent human studies have associated immunotherapy response with increased intratumoral B cell diversity.[25] The presence of tertiary lymphoid structures consisting of organized collections of T, B, and dendritic cells, where immune cell education and activation against tumor antigens is hypothesized to occur, has been shown to confer improved response to these therapies.[23–25] Furthermore, murine tumor modeling supports a central functional role for B cells in immune interactions occurring in the context of PD-1 pathway blockade.[46] Additional mechanistic studies integrating this knowledge to B cell functional diversity in the tumor microenvironment will be required to elucidate the functional contributions of these processes to anti-tumor immunity.

Moving forward, we envision machine learning approaches that are not limited to integration of static features of pre-treatment tumors but also encompass dynamic biomarkers that capture tumor and immune response evolution under the selective pressure of immune-targeted therapies.

Limitations of Study

Our work on integrative modeling of multi-omics sequence data is limited by the relatively small sample size and heterogeneity of the cohort analyzed. Additional larger scale studies of prospectively collected cohorts would be necessary to independently validate the predictive value of our multi-modal approach.

STAR★METHODS

Detailed methods are provided in the online version of this paper and include the following:

- KEY RESOURCES TABLE
- RESOURCE AVAILABILITY
  - Lead Contact
  - Materials availability
  - Data and Code Availability
- EXPERIMENTAL MODEL AND SUBJECT DETAILS
  - Patient characteristics and treatment
  - Assessment of clinical response
- METHOD DETAILS
  - Tissue sample characteristics
  - Whole exome sequencing
  - Mutation Signature Analysis
  - Copy number analysis, tumor **purity, ploidy and clonality** assessment
  - HLA class I and II genetic variation and loss of heterozygosity
  - RNA sequencing pipeline and analysis
  - TCR sequencing
  - B cell receptor analyses
  - Morphological assessment of plasma cells
  - Modeling of tumor dynamics during therapy
  - Machine learning
- QUANTIFICATION AND STATISTICAL ANALYSIS
- ADDITIONAL RESOURCES

SUPPLEMENTAL INFORMATION

Supplemental Information can be found online at https://doi.org/10.1016/j.xcrm.2020.100139.

ACKNOWLEDGMENTS

We thank members of our labs for critical review of the manuscript. This work was supported by Bristol-Myers Squibb and in part by US National Institutes of Health grants CA121113 (V.E.V. and V.A.), CA233259 (V.E.V.), CA006973 (V.E.V.), CA142779 (S.L.T., J.T., and D.P.M.) and CA233259 (V.E.V.); the Commonwealth Foundation (V.E.V.); the Bloomberg-Kimmel Institute for Cancer Immunotherapy (V.A., J.T., D.M.P., S.L.T., and V.E.V.); the Dr. Miriam and Sheldon G. Adelson Medical Research Foundation (V.E.V.); the V Foundation (V.A. and V.E.V.); Swim Across America (V.A.); the Allegheny Health Network – Johns Hopkins Research Fund (V.A. and V.E.V.); the LUNGevity Foundation (V.A.); the Mark Foundation For Cancer Research (V.E.V. and J.T.); the Barney Foundation (J.T. and S.L.T.); Moving for Melanoma of Delaware (J.T. and S.L.T.); the Laverna Hahn Charitable Trust (J.T. and S.L.T.); the Melanoma Research Alliance (J.T., A.R., D.M.P., and S.L.T.); and a Cancer Immunology

Translational Cancer Research Grant (SU2C-AACR-DT1012) from Cancer Research Institute–Stand Up 2 Cancer (J.T., A.R., D.M.P., and S.L.T.). Stand Up 2 Cancer is a program of the Entertainment Industry Foundation administered by the American Association for Cancer Research.

AUTHOR CONTRIBUTIONS

Conceptualization, V.A., S.L.T., and V.E.V.; Methodology, V.A., D.C.B., N.N., J.R.W., X.M.S., and V.E.V.; Software, D.C.B., N.N., J.R.W., X.M.S., and A.B.; Formal Analysis, V.A., D.C.B., N.N., J.R.W., A.B., L.F., R.K., and R.B.S.; Resources, P.R.-M. and M.W.-R.; Data Curation, P.R.-M. and M.W.-R.; Writing – Original Draft, V.A., D.C.B., J.W.S., Z.B., J.M., A.S.B., C.G., A.R., D.M.P., S.L.T., and V.E.V.; Visualization, V.A., D.C.B., N.N., and J.R.W.; Supervision, V.A., S.L.T., and V.E.V.; Funding Acquisition, V.A., S.L.T., and V.E.V.

DECLARATION OF INTERESTS

V.A. and J.T. receive research funding from Bristol-Myers Squibb. J.T. serves as a consultant/advisory board member to Bristol-Myers Squibb, Merck, Astra Zeneca, and Compugen. J.R.W. is a consultant for Personal Genome Diagnostics; is the founder and owner of Resphera Biosciences; and holds patents, royalties, or other intellectual property from Personal Genomic Diagnostics. A.B. receives honoraria from Proscia and Corista; is a consultant of Bristol-Myers Squibb, Genentech, and Bayer; and receives research funding from Genentech. C.G. has patents, royalties, or other intellectual property from Karyopharm and Arcus. A.R. has received honoraria from consulting with Amgen, Bristol-Myers Squibb, Chugai, Genentech, Merck, Novartis, Roche, and Sanofi; is or has been a member of the scientific advisory board and holds stock in Advaxis, Arcus Biosciences, Bioncotech Therapeutics, Compugen, CytomX, Five Prime, FLX-Bio, ImaginAb, Isoplexis, Kite-Gilead, Lutris Pharma, Merus, PACT Pharma, Rgenix, and Tango Therapeutics; and has received research funding from Agilent and from Bristol-Myers Squibb through Stand Up to Cancer (SU2C). P.R.-M. and M.W.-R. are employees of Bristol-Myers Squibb. D.M.P. and S.L.T. report stock and other ownership interests in Aduro Biotech, DNAtrix, Dracen Pharmaceuticals, Dragonfly Therapeutics, Ervaxx, Five Prime Therapeutics, Potenza Therapeutics, RAPT, Tizona Therapeutics, Trieza Therapeutics, and WindMIL; a consulting or advisory role in Amgen, DNAtrix, Dragonfly Therapeutics, Dynavax, Ervaxx, Five Prime Therapeutics, Immunocore, Immunomic Therapeutics, Janssen Pharmaceuticals, MedImmune/AstraZeneca, Merck, RAPT, and WindMIL; research grants from Bristol-Myers Squibb and Compugen; patents, royalties, and/or other intellectual property through their institution with Aduro Biotech, Arbor Pharmaceuticals, Bristol-Myers Squibb, Immunomic Therapeutics, NexImmune, and WindMIL; and travel, accommodations, and expenses from Bristol-Myers Squibb and Five Prime Therapeutics. V.E.V. is a founder of Delfi Diagnostics and Personal Genome Diagnostics, serves on the Board of Directors and as a consultant for both organizations, and owns Delfi Diagnostics and Personal Genome Diagnostics stock, which are subject to certain restrictions under university policy. Additionally, Johns Hopkins University owns equity in Delfi Diagnostics and Personal Genome Diagnostics. V.E.V. is an advisor to Bristol-Myers Squibb, Genentech, Merck, and Takeda Pharmaceuticals. Within the last 5 years, V.E.V. has been an advisor to Daiichi Sankyo, Janssen Diagnostics, and Ignyta. These arrangements have been reviewed and approved by the Johns Hopkins University in accordance with its conflict of interest policies.

Received: June 24, 2020
Revised: August 10, 2020
Accepted: October 20, 2020
Published: November 17, 2020

REFERENCES

1. Larkin, J., Chiarion-Sileni, V., Gonzalez, R., Grob, J.J., Cowey, C.L., Lao, C.D., Schadendorf, D., Dummer, R., Smylie, M., Rutkowski, P., et al. (2015). Combined nivolumab and ipilimumab or monotherapy in untreated melanoma. N. Engl. J. Med. *373*, 23–34.
2. Larkin, J., Chiarion-Sileni, V., Gonzalez, R., Grob, J.J., Rutkowski, P., Lao, C.D., Cowey, C.L., Schadendorf, D., Wagstaff, J., Dummer, R., et al. (2019). Five-year survival with combined nivolumab and ipilimumab in advanced melanoma. N. Engl. J. Med. *381*, 1535–1546.
3. Snyder Charen, A., Makarov, V., Merghoub, T., Walsh, L., Yuan, J., Miller, M., Kannan, K., Postow, M.A., Elipenahli, C., Liu, C., et al. (2014). The neoantigen landscape underlying clinical response to ipilimumab. J. Clin. Oncol. *32*, 3003.
4. Liu, D., Schilling, B., Liu, D., Sucker, A., Livingstone, E., Jerby-Arnon, L., Zimmer, L., Gutzmer, R., Satzger, I., Loquai, C., et al. (2019). Integrative molecular and clinical modeling of clinical outcomes to PD1 blockade in patients with metastatic melanoma. Nat. Med. *25*, 1916–1927.
5. Samstein, R.M., Lee, C.H., Shoushtari, A.N., Hellmann, M.D., Shen, R., Janjigian, Y.Y., Barron, D.A., Zehir, A., Jordan, E.J., Omuro, A., et al. (2019). Tumor mutational load predicts survival after immunotherapy across multiple cancer types. Nat. Genet. *51*, 202–206.
6. Van Allen, E.M., Miao, D., Schilling, B., Shukla, S.A., Blank, C., Zimmer, L., Sucker, A., Hillen, U., Foppen, M.H.G., Goldinger, S.M., et al. (2015). Genomic correlates of response to CTLA-4 blockade in metastatic melanoma. Science *350*, 207–211.
7. Davoli, T., Uno, H., Wooten, E.C., and Elledge, S.J. (2017). Tumor aneuploidy correlates with markers of immune evasion and with reduced response to immunotherapy. Science *355*, eaaf8399.
8. Zaretsky, J.M., Garcia-Diaz, A., Shin, D.S., Escuin-Ordinas, H., Hugo, W., Hu-Lieskovan, S., Torrejon, D.Y., Abril-Rodriguez, G., Sandoval, S., Barthly, L., et al. (2016). Mutations associated with acquired resistance to PD-1 blockade in melanoma. N. Engl. J. Med. *375*, 819–829.
9. Peng, W., Chen, J.Q., Liu, C., Malu, S., Creasy, C., Tetzlaff, M.T., Xu, C., McKenzie, J.A., Zhang, C., Liang, X., et al. (2016). Loss of PTEN promotes resistance to T cell-mediated immunotherapy. Cancer Discov. *6*, 202–216.
10. Anagnostou, V., Smith, K.N., Forde, P.M., Niknafs, N., Bhattacharya, R., White, J., Zhang, T., Adleff, V., Phallen, J., Wali, N., et al. (2017). Evolution of neoantigen landscape during immune checkpoint blockade in non-small cell lung cancer. Cancer Discov. *7*, 264–276.
11. Sade-Feldman, M., Jiao, Y.J., Chen, J.H., Rooney, M.S., Barzily-Rokni, M., Eliane, J.P., Bjorgaard, S.L., Hammond, M.R., Vitzthum, H., Blackmon, S.M., et al. (2017). Resistance to checkpoint blockade therapy through inactivation of antigen presentation. Nat. Commun. *8*, 1136.
12. Spranger, S., Bao, R., and Gajewski, T.F. (2015). Melanoma-intrinsic β-catenin signalling prevents anti-tumour immunity. Nature *523*, 231–235.
13. Grasso, C.S., Giannakis, M., Wells, D.K., Hamada, T., Mu, X.J., Quist, M., Nowak, J.A., Nishihara, R., Qian, Z.R., Inamura, K., et al. (2018). Genetic mechanisms of immune evasion in colorectal cancer. Cancer Discov. *8*, 730–749.
14. Patel, S.J., Sanjana, N.E., Kishton, R.J., Eidizadeh, A., Vodnala, S.K., Cam, M., Gartner, J.J., Jia, L., Steinberg, S.M., Yamamoto, T.N., et al. (2017). Identification of essential genes for cancer immunotherapy. Nature *548*, 537–542.
15. Tumeh, P.C., Harview, C.L., Yearley, J.H., Shintaku, I.P., Taylor, E.J., Robert, L., Chmielowski, B., Spasic, M., Henry, G., Ciobanu, V., et al. (2014). PD-1 blockade induces responses by inhibiting adaptive immune resistance. Nature *515*, 568–571.
16. Riaz, N., Havel, J.J., Makarov, V., Desrichard, A., Urba, W.J., Sims, J.S., Hodi, F.S., Martín-Algarra, S., Mandal, R., Sharfman, W.H., et al. (2017). Tumor and microenvironment evolution during immunotherapy with nivolumab. Cell *171*, 934–949.e16.
17. Sade-Feldman, M., Yizhak, K., Bjorgaard, S.L., Ray, J.P., de Boer, C.G., Jenkins, R.W., Lieb, D.J., Chen, J.H., Frederick, D.T., Barzily-Rokni, M., et al. (2018). Defining T cell states associated with response to checkpoint immunotherapy in melanoma. Cell *175*, 998–1013.e20.
18. Wolf, Y., Bartok, O., Patkar, S., Eli, G.B., Cohen, S., Litchfield, K., Levy, R., Jiménez-Sánchez, A., Trabish, S., Lee, J.S., et al. (2019). UVB-induced

tumor heterogeneity diminishes immune response in melanoma. Cell *179*, 219–235.e21.

19. Anagnostou, V., Niknafs, N., Marrone, K., Bruhm, D.C., White, J.R., Naidoo, J., Hummelink, K., Monkhorst, K., Lalezari, F., Lanis, M., et al. (2020). Multimodal genomic features predict outcome of immune checkpoint blockade in non-small cell lung cancer. Nature Cancer *1*, 99–111.
20. Cristescu, R., Mogg, R., Ayers, M., Albright, A., Murphy, E., Yearley, J., Sher, X., Liu, X.Q., Lu, H., Nebozhyn, M., et al. (2018). Pan-tumor genomic biomarkers for PD-1 checkpoint blockade-based immunotherapy. Science *362*, eaar3593.
21. Chen, P.L., Roh, W., Reuben, A., Cooper, Z.A., Spencer, C.N., Prieto, P.A., Miller, J.P., Bassett, R.L., Gopalakrishnan, V., Wani, K., et al. (2016). Analysis of immune signatures in longitudinal tumor samples yields insight into biomarkers of response and mechanisms of resistance to immune checkpoint blockade. Cancer Discov. *6*, 827–837.
22. Griss, J., Bauer, W., Wagner, C., Simon, M., Chen, M., Grabmeier-Pfistershammer, K., Maurer-Granofszky, M., Roka, F., Penz, T., Bock, C., et al. (2019). B cells sustain inflammation and predict response to immune checkpoint blockade in human melanoma. Nat. Commun. *10*, 4186.
23. Petitprez, F., de Reyniès, A., Keung, E.Z., Chen, T.W., Sun, C.M., Calderaro, J., Jeng, Y.M., Hsiao, L.P., Lacroix, L., Bougoüin, A., et al. (2020). B cells are associated with survival and immunotherapy response in sarcoma. Nature *577*, 556–560.
24. Cabrita, R., Lauss, M., Sanna, A., Donia, M., Skaarup Larsen, M., Mitra, S., Johansson, I., Phung, B., Harbst, K., Vallon-Christersson, J., et al. (2020). Tertiary lymphoid structures improve immunotherapy and survival in melanoma. Nature *577*, 561–565.
25. Helmink, B.A., Reddy, S.M., Gao, J., Zhang, S., Basar, R., Thakur, R., Yizhak, K., Sade-Feldman, M., Blando, J., Han, G., et al. (2020). B cells and tertiary lymphoid structures promote immunotherapy response. Nature *577*, 549–555.
26. Sumimoto, H., Imabayashi, F., Iwata, T., and Kawakami, Y. (2006). The BRAF-MAPK signaling pathway is essential for cancer-immune evasion in human melanoma cells. J. Exp. Med. *203*, 1651–1656.
27. Wolchok, J.D., Chiarion-Sileni, V., Gonzalez, R., Rutkowski, P., Grob, J.J., Cowey, C.L., Lao, C.D., Wagstaff, J., Schadendorf, D., Ferrucci, P.F., et al. (2017). Overall survival with combined nivolumab and ipilimumab in advanced melanoma. N. Engl. J. Med. *377*, 1345–1356.
28. Zhang, Z., Jones, A.E., Wu, W., Kim, J., Kang, Y., Bi, X., Gu, Y., Popov, I.K., Renfrow, M.B., Vassylyeva, M.N., et al. (2017). Role of remodeling and spacing factor 1 in histone H2A ubiquitination-mediated gene silencing. Proc. Natl. Acad. Sci. USA *114*, E7949–E7958.
29. Chowell, D., Krishna, C., Pierini, F., Makarov, V., Rizvi, N.A., Kuo, F., Morris, L.G.T., Riaz, N., Lenz, T.L., and Chan, T.A. (2019). Evolutionary divergence of HLA class I genotype impacts efficacy of cancer immunotherapy. Nat. Med. *25*, 1715–1720.
30. Wherry, E.J., and Kurachi, M. (2015). Molecular and cellular insights into T cell exhaustion. Nat. Rev. Immunol. *15*, 486–499.
31. Khan, O., Giles, J.R., McDonald, S., Manne, S., Ngiow, S.F., Patel, K.P., Werner, M.T., Huang, A.C., Alexander, K.A., Wu, J.E., et al. (2019). TOX transcriptionally and epigenetically programs $CD8^+$ T cell exhaustion. Nature *571*, 211–218.
32. Newman, A.M., Liu, C.L., Green, M.R., Gentles, A.J., Feng, W., Xu, Y., Hoang, C.D., Diehn, M., and Alizadeh, A.A. (2015). Robust enumeration of cell subsets from tissue expression profiles. Nat. Methods *12*, 453–457.
33. Hu, X., Zhang, J., Wang, J., Fu, J., Li, T., Zheng, X., Wang, B., Gu, S., Jiang, P., Fan, J., et al. (2019). Landscape of B cell immunity and related immune evasion in human cancers. Nat. Genet. *51*, 560–567.
34. Rizvi, H., Sanchez-Vega, F., La, K., Chatila, W., Jonsson, P., Halpenny, D., Plodkowski, A., Long, N., Sauter, J.L., Rekhtman, N., et al. (2018). Molecular determinants of response to anti-programmed cell death (PD)-1 and anti-programmed death-ligand 1 (PD-L1) blockade in patients with non-small-cell lung cancer profiled with targeted next-generation sequencing. J. Clin. Oncol. *36*, 633–641.
35. Jiang, P., Gu, S., Pan, D., Fu, J., Sahu, A., Hu, X., Li, Z., Traugh, N., Bu, X., Li, B., et al. (2018). Signatures of T cell dysfunction and exclusion predict cancer immunotherapy response. Nat. Med. *24*, 1550–1558.
36. Hugo, W., Zaretsky, J.M., Sun, L., Song, C., Moreno, B.H., Hu-Lieskovan, S., Berent-Maoz, B., Pang, J., Chmielowski, B., Cherry, G., et al. (2016). Genomic and transcriptomic features of response to anti-PD-1 therapy in metastatic melanoma. Cell *165*, 35–44.
37. Auslander, N., Zhang, G., Lee, J.S., Frederick, D.T., Miao, B., Moll, T., Tian, T., Wei, Z., Madan, S., Sullivan, R.J., et al. (2018). Robust prediction of response to immune checkpoint blockade therapy in metastatic melanoma. Nat. Med. *24*, 1545–1549.
38. Lee, J.H., Shklovskaya, E., Lim, S.Y., Carlino, M.S., Menzies, A.M., Stewart, A., Pedersen, B., Irvine, M., Alavi, S., Yang, J.Y.H., et al. (2020). Transcriptional downregulation of MHC class I and melanoma de- differentiation in resistance to PD-1 inhibition. Nat. Commun. *11*, 1897.
39. Zhang, J., Ji, Z., Caushi, J.X., El Asmar, M., Anagnostou, V., Cottrell, T.R., Chan, H.Y., Suri, P., Guo, H., Merghoub, T., et al. (2020). Compartmental analysis of T-cell clonal dynamics as a function of pathologic response to neoadjuvant PD-1 blockade in resectable non-small cell lung cancer. Clin. Cancer Res. *26*, 1327–1337.
40. Anagnostou, V., Forde, P.M., White, J.R., Niknafs, N., Hruban, C., Naidoo, J., Marrone, K., Sivakumar, I.K.A., Bruhm, D.C., Rosner, S., et al. (2019). Dynamics of tumor and immune responses during immune checkpoint blockade in non-small cell lung cancer. Cancer Res. *79*, 1214–1225.
41. Grasso, C.S., Tsoi, J., Onyshchenko, M., Abril-Rodriguez, G., Ross-Macdonald, P., Wind-Rotolo, M., Champhekar, A., Medina, E., Torrejon, D.Y., Shin, D.S., et al. (2020). Conserved interferon-γ signaling drives clinical response to immune checkpoint blockade therapy in melanoma. Cancer Cell *38*, 500–515.e3.
42. Yuan, J., Adamow, M., Ginsberg, B.A., Rasalan, T.S., Ritter, E., Gallardo, H.F., Xu, Y., Pogoriler, E., Terzulli, S.L., Kuk, D., et al. (2011). Integrated NY-ESO-1 antibody and CD8+ T-cell responses correlate with clinical benefit in advanced melanoma patients treated with ipilimumab. Proc. Natl. Acad. Sci. USA *108*, 16723–16728.
43. Damsky, W., Jilaveanu, L., Turner, N., Perry, C., Zito, C., Tomayko, M., Leventhal, J., Herold, K., Meffre, E., Bosenberg, M., and Kluger, H.M. (2019). B cell depletion or absence does not impede anti-tumor activity of PD-1 inhibitors. J. Immunother. Cancer *7*, 153.
44. Zhong, G., Reis e Sousa, C., and Germain, R.N. (1997). Antigen-unspecific B cells and lymphoid dendritic cells both show extensive surface expression of processed antigen-major histocompatibility complex class II complexes after soluble protein exposure in vivo or in vitro. J. Exp. Med. *186*, 673–682.
45. Crawford, A., Macleod, M., Schumacher, T., Corlett, L., and Gray, D. (2006). Primary T cell expansion and differentiation in vivo requires antigen presentation by B cells. J. Immunol. *176*, 3498–3506.
46. Hollern, D.P., Xu, N., Thennavan, A., Glodowski, C., Garcia-Recio, S., Mott, K.R., He, X., Garay, J.P., Carey-Ewend, K., Marron, D., et al. (2019). B cells and T follicular helper cells mediate response to checkpoint inhibitors in high mutation burden mouse models of breast cancer. Cell *179*, 1191–1206.e21.
47. Jones, S., Anagnostou, V., Lytle, K., Parpart-Li, S., Nesselbush, M., Riley, D.R., Shukla, M., Chesnick, B., Kadan, M., Papp, E., et al. (2015). Personalized genomic analyses for cancer mutation discovery and interpretation. Sci. Transl. Med. *7*, 283ra53.
48. Shao, X.M., Bhattacharya, R., Huang, J., Sivakumar, I.K.A., Tokheim, C., Zheng, L., Hirsch, D., Kaminow, B., Omdahl, A., Bonsack, M., et al. (2020). High-throughput prediction of MHC class I and II neoantigens with MHCnuggets. Cancer Immunol. Res. *8*, 396–408.
49. Ghorani, E., Rosenthal, R., McGranahan, N., Reading, J.L., Lynch, M., Peggs, K.S., Swanton, C., and Quezada, S.A. (2018). Differential binding

affinity of mutated peptides for MHC class I is a predictor of survival in advanced lung cancer and melanoma. Ann. Oncol. *29*, 271–279.

50. Rosenthal, R. (2016). deconstructSigs: identifies signatures present in a tumor sample. https://cran.r-project.org/web/packages/deconstructSigs/index.html.
51. Niknafs, N., Beleva-Guthrie, V., Naiman, D.Q., and Karchin, R. (2015). SubClonal hierarchy inference from somatic mutations: automatic reconstruction of cancer evolutionary trees from multi-region next generation sequencing. PLoS Comput. Biol. *11*, e1004416.
52. Szolek, A., Schubert, B., Mohr, C., Sturm, M., Feldhahn, M., and Kohlbacher, O. (2014). OptiType: precision HLA typing from next-generation sequencing data. Bioinformatics *30*, 3310–3316.
53. Xie, C., Yeo, Z.X., Wong, M., Piper, J., Long, T., Kirkness, E.F., Biggs, W.H., Bloom, K., Spellman, S., Vierra-Green, C., et al. (2017). Fast and accurate HLA typing from short-read next-generation sequence data with xHLA. Proc. Natl. Acad. Sci. USA *114*, 8059–8064.
54. Cao, H., Wu, J., Wang, Y., Jiang, H., Zhang, T., Liu, X., Xu, Y., Liang, D., Gao, P., Sun, Y., et al. (2013). An integrated tool to study MHC region: accurate SNV detection and HLA genes typing in human MHC region using targeted high-throughput sequencing. PLoS ONE *8*, e69388.
55. Shukla, S.A., Rooney, M.S., Rajasagi, M., Tiao, G., Dixon, P.M., Lawrence, M.S., Stevens, J., Lane, W.J., Dellagatta, J.L., Steelman, S., et al. (2015). Comprehensive analysis of cancer-associated somatic mutations in class I HLA genes. Nat. Biotechnol. *33*, 1152–1158.
56. McGranahan, N., Rosenthal, R., Hiley, C.T., Rowan, A.J., Watkins, T.B.K., Wilson, G.A., Birkbak, N.J., Veeriah, S., Van Loo, P., Herrero, J., et al. (2017). Allele-specific HLA loss and immune escape in lung cancer evolution. Cell *171*, 1259–1271.e11.
57. Bolger, A.M., Lohse, M., and Usadel, B. (2014). Trimmomatic: a flexible trimmer for Illumina sequence data. Bioinformatics *30*, 2114–2120.
58. Dobin, A., Davis, C.A., Schlesinger, F., Drenkow, J., Zaleski, C., Jha, S., Batut, P., Chaisson, M., and Gingeras, T.R. (2013). STAR: ultrafast universal RNA-seq aligner. Bioinformatics *29*, 15–21.
59. Li, B., and Dewey, C.N. (2011). RSEM: accurate transcript quantification from RNA-seq data with or without a reference genome. BMC Bioinformatics *12*, 323.
60. Haas, B.J., Dobin, A., Li, B., Stransky, N., Pochet, N., and Regev, A. (2019). Accuracy assessment of fusion transcript detection via read-mapping and de novo fusion transcript assembly-based methods. Genome Biol. *20*, 213.
61. Fu, J., Li, K., Zhang, W., Wan, C., Zhang, J., Jiang, P., and Liu, X.S. (2020). Large-scale public data reuse to model immunotherapy response and resistance. Genome Med. *12*, 21.
62. Carlson, C.S., Emerson, R.O., Sherwood, A.M., Desmarais, C., Chung, M.W., Parsons, J.M., Steen, M.S., LaMadrid-Herrmannsfeldt, M.A., Williamson, D.W., Livingston, R.J., et al. (2013). Using synthetic templates to design an unbiased multiplex PCR assay. Nat. Commun. *4*, 2680.
63. Bolotin, D.A., Poslavsky, S., Mitrophanov, I., Shugay, M., Mamedov, I.Z., Putintseva, E.V., and Chudakov, D.M. (2015). MiXCR: software for comprehensive adaptive immunity profiling. Nat. Methods *12*, 380–381.
64. Burkner, P.-C. (2017). brms: an R package for Bayesian multilevel models using Stan. J. Stat. Softw. *80*, 1–28.

STAR★METHODS

KEY RESOURCES TABLE

REAGENT or RESOURCE	SOURCE	IDENTIFIER
Biological Samples		
Tumor tissue from participants in the CheckMate 038 clinical trial	CheckMate 038	CheckMate-038 clinical trial (NCT01621490) https://clinicaltrials.gov/ct2/show/results/NCT01621490
Deposited Data		
Whole exome sequence data	This paper	EGAS00001004548
RNA sequencing data	This paper	EGAS00001004545
Software and Algorithms		
VariantDx	Jones et al.[47]	N/A
Immuno*Select*-R	Personal Genome Diagnostics	N/A
MHCnuggets	Shao et al.[48]	https://github.com/KarchinLab/mhcnuggets
deconstructSigs	Rosenthal[50]	https://github.com/raerose01/deconstructSigs
SCHISM	Niknafs et al.[51]	https://github.com/KarchinLab/SCHISM
OptiType	Szolek et al.[52]	https://github.com/FRED-2/OptiType
xHLA	Xie et al.[53]	https://github.com/humanlongevity/HLA
SOAP-HLA	Cao et al.[54]	https://github.com/adefelicibus/soap-hla
POLYSOLVER	Shukla et al.[55]	https://software.broadinstitute.org/cancer/cga/polysolver
LOHHLA	McGranahan et al.[56]	https://bitbucket.org/mcgranahanlab/lohhla/src/master/
Trimmomatic	Bolger et al.[57]	http://www.usadellab.org/cms/index.php?page=trimmomatic
STAR	Dobin et al.[58]	https://github.com/alexdobin/STAR
Picard Tools	Broad Institute	https://broadinstitute.github.io/picard/
RSEM	Li and Dewey[59]	https://github.com/deweylab/RSEM
STAR-Fusion	Haas et al.[60]	https://github.com/STAR-Fusion/STAR-Fusion
CIBERSORT	Newman et al.[32]	https://cibersort.stanford.edu/
TIDE	Fu et al.[61]	http://tide.dfci.harvard.edu/
TRUST	Hu et al.[33]	https://github.com/liulab-dfci/TRUST4
MiXCR	Bolotin et al.[63]	https://github.com/milaboratory/mixcr
brms	Burkner[64]	https://github.com/paul-buerkner/brms
randomForest		https://cran.rstudio.com/web/packages/randomForest/
caret		https://cran.r-project.org/web/packages/caret/
ROCR		https://cran.r-project.org/web/packages/ROCR/
survminer		https://github.com/kassambara/survminer
survival		https://github.com/therneau/survival
coin		http://coin.r-forge.r-project.org
SPSS	IBM	N/A
R	R Core Team	https://www.r-project.org/

RESOURCE AVAILABILITY

Lead Contact

Further information and requests for resources should be directed to and will be fulfilled by the Lead Contact, Victor Velculescu (velculescu@jhmi.edu).

Materials availability

This study did not generate new unique reagents.

Data and Code Availability

The accession numbers for WES and RNaseq sequence data reported in this paper from patients who consented to sequence data deposition are EGAS00001004548 and EGAS00001004545 (deposited in the European Genome phenome Archive).

EXPERIMENTAL MODEL AND SUBJECT DETAILS

Patient characteristics and treatment

CheckMate 038 was a prospective, multicenter, international, multi-cohort clinical trial of nivolumab as front-line therapy (Part 3 arm B and part 4 arm E) or after progressing on therapy with the anti-CTLA-4 antibody ipilimumab (part 1), or receiving the combination of both antibodies (Parts 2 and 3 arm A and part 4 arm D, NCT01621490) A full description of the clinical trials and its outcomes can be found at https://clinicaltrials.gov/ct2/show/results/NCT01621490. Analyses of CheckMate 038 part 1[16] and parts 1-4[41] that included detailed descriptions of the cohorts in each arm have been previously published. The clinical trial protocol and its amendments were approved by the relevant institutional review boards, and the study was conducted in accordance with the Declaration of Helsinki and the International Conference on Harmonization Guidelines for Good Clinical Practice. All patients signed written informed consent prior to having any study procedures performed. Here, we analyzed biopsies of patients in CheckMate 038 parts 2-4 and patient characteristics are summarized in Table S1A.

Assessment of clinical response

Radiographic assessment of response was performed approximately every 8 weeks until progression and disease progression was confirmed with a repeat CT scan at least four weeks later. Response to therapy indicates best overall response by response evaluation criteria in solid tumors (RECIST) 1.1. Patients with complete (CR) and partial (PR) response as BOR were classified as responders while patients with stable (SD) or progressive disease (PD) were classified as non-responders. PFS and OS were defined as the time from treatment initiation to documented evidence of progressive disease or death. Radiographic responses and outcome are listed in Table S1A.

METHOD DETAILS

Tissue sample characteristics

Patients underwent a baseline biopsy prior to therapy initiation (1 to 7 days before the first dose of therapy) and a repeat biopsy, 2-4 weeks on-therapy. Tumor tissue was stored in RNAlater (TheromoFisher, MA) for subsequent RNA/DNA extraction.

Whole exome sequencing

Sample preparation

Whole exome sequencing was performed on pre-treatment tumor and matched normal samples. DNA was extracted from patients' tumors and matched peripheral blood using the QIAGEN DNA kit (QIAGEN, CA). Fragmented genomic DNA from tumor and normal samples was used for Illumina TruSeq library construction (Illumina, San Diego, CA) and exonic regions were captured in solution using the Agilent SureSelect v.4 kit (Agilent, Santa Clara, CA) according to the manufacturers' instructions as previously described[10,47]. Paired-end sequencing, resulting in 100 bases from each end of the fragments for the exome libraries was performed using Illumina HiSeq 2000/2500 instrumentation (Illumina, San Diego, CA). The mean depth of total and distinct coverage for the pre-treatment tumors were 206x and 173x (Table S1O).

Mutation calling

Somatic mutations, consisting of point mutations, insertions, and deletions across the whole exome were identified using the VariantDx custom software for identifying mutations in matched tumor and normal samples as previously described (Personal Genome Diagnostics, Baltimore, MD)[10,47]. Somatic sequence alterations are listed in Table S1B.

Computational neoantigen prediction

Somatic mutations, consisting of nonsynonymous single base substitutions, insertions and deletions, were evaluated for putative MHC class I neoantigens using the Immuno*Select*-R pipeline (Personal Genome Diagnostics, Baltimore, MD) as previously described[10]. We employed MHCnuggets[48] to analyze MHC class II neoantigens. In brief, for each single-base substitution mutation, mutant and reference peptide sequences surrounding the affected amino acid were extracted, filtering out silent and none sense mutations. Windowing around the affected amino acid, all possible 12-20-mer mutant/reference peptide pairs were then selected as candidate neoantigens. Each patient's candidate neoantigens were then predicted against the patient's MHC II haplotypes. Putative immunogenic peptides were defined as candidate mutant peptides with an $IC_{50} < 500nM$ and a differential agretopic index (DAI), defined as $= \frac{Reference\ Peptide\ IC50}{Mutant\ Peptide\ IC50}$[49], higher than 2.

Mutation Signature Analysis

Mutation signatures were derived based on the fraction of coding point mutations in each of 96 trinucleotide contexts and estimated the contribution of each signature to each tumor sample using the deconstructSigs R package[50].

Copy number analysis, tumor purity, ploidy and clonality assessment

The somatic copy number profile and the extent of aneuploidy in each tumor were estimated using whole exome sequencing data as previously described[19]. Focal copy number alterations are summarized in Table S1E. We calculated several measures of tumor aneuploidy including the fraction of the genome with loss of heterozygosity (LOH that signifies complete loss of the minor allele), and allelic imbalance (AI that denotes inequality of major and minor allele copy number; Table S1F). Mutant allele frequency, ploidy and purity were incorporated to estimate mutation cellular fraction, that is the fraction of cancer cells that harbor a specific mutation, as previously described[19,51].

HLA class I and II genetic variation and loss of heterozygosity

OptiType v1.2. was used to determine HLA class I haplotypes[52], xHLA was used to determine HLA class II haplotypes for HLA-DPB1, HLA-DQB1, HLA-DRB1[53], and SOAP-HLA was used to determined class II haplotypes for HLA-DPA1 and HLA-DQA1[54]. A separate bioinformatic analysis using POLYSOLVER[55] was applied to detect and annotate the somatic mutations in class I HLA genes. Loss of heterozygosity of each HLA gene was determined by considering the minor allele copy number of the overlapping genomic region (minor CN = 0 indicated complete loss of minor allele). We determined HLA class I loss in the tumor by applying LOHHLA using default program settings[56]. For two patients, 20039 and 30019, class I HLA loss was not identified by LOHHLA but was identified manually by the presence of LOH through analysis of allele-specific copy number at this locus. The number of unique class I HLA alleles in the tumor was calculated by subtracting the number of germline heterozygous alleles with somatic LOH from the total number of unique alleles in germline. Germline and somatic HLA class I genomic variation is summarized in Table S1G. We evaluated somatic loss of class II HLA genes by review of allele-specific copy number of these loci, where minor copy number of zero indicated loss of heterozygosity. The number of unique class II HLA genes in the germline and the tumor was calculated similar to class I HLA genes, and is summarized in Table S1G.

RNA sequencing pipeline and analysis

Paired-end reads were first processed to remove adapters and low quality sequences using Trimmomatic v0.36[57]. Reads were then aligned to the GRCh37 reference genome using STAR v2.5.1b[58] and duplicate reads were filtered using Picard Tools (https://broadinstitute.github.io/picard/). RNA sequencing characteristics are summarized in Table S1P. Normalized gene-level expression measurements were then obtained as transcripts per million (TPM) with RSEM v1.2.30 using the strand-specific mode[59]. STAR-Fusion v1.2.0[60] was utilized to identify somatic and immunoglobulin rearrangements. CIBERSORT v1.06 was used for deconvolution of transcriptome data to generate relative proportion estimates for 22 immune cell types[32]. CIBERSORT determines the fraction of each immune cell type among the total immune cells in the mixture and we employed the relative abundance measurement of immune cell subsets for differential abundance analyses as opposed to the absolute abundance metrics. Single base substitutions identified through whole-exome sequencing were considered expressed if at least 3 reads containing the mutation were detected by RNaseq (Table S1C). When explicitly stated, gene expression measurements were normalized to control for the degree of leukocytic intratumoral infiltration by dividing their expression by the expression of the LCA gene. The TIDE algorithm was implemented[35], using TPM values, where a log2 fold change was computed for each gene in each sample relative to the average expression of that gene across 41 samples with baseline RNaseq data. The resulting matrix was used as input to compute the TIDE score using the TIDE web platform[61].

TCR sequencing

TCR clones were evaluated in tumor tissue by next generation sequencing, with an input material of 500ng of genomic DNA for each sample analyzed. TCR-β CDR3 regions were amplified using the survey ImmunoSeq assay in a multiplex PCR method using 45 forward primers specific to TCR Vβ gene segments and 13 reverse primers specific to TCR Jβ gene segments (Adaptive Biotechnologies)[62]. Productive TCR sequences were further analyzed (Table S1H). For each sample, a clonality metric was estimated in order to quantitate the extent of mono- or oligo-clonal expansion by measuring the shape of the clone frequency distribution. Clonality values range from 0 to 1, where values approaching 1 indicate a nearly monoclonal population (Table S1H). For differential abundance analysis between baseline and on-therapy tumors, we selected the most expanded and most regressed TCR clonotypes, corresponding to fold changes in productive frequency of TCR clones with an FDR < 0.001. These TCR clones are referred to as expanded and regressed.

B cell receptor analyses

IgH and IgL CRD3 assemblies and IgH isotypes were generated by running TRUST[33] and MiXCR[63] using RNaseq FASTQ files as input. For each sample, the productive BCR clone count and the BCR repertoire clonality were calculated utilizing IgH CDR3 sequences. BCR clonality was defined as (1-normalized Shannon entropy), where normalized Shannon entropy is Shannon entropy/log2(unique productive clones). For differential abundance analysis between baseline and on-therapy tumors, BCR clonotypes with a fold change in productive frequencies between baseline and on-treatment tumors with an FDR < 0.05 we considered.

Morphological assessment of plasma cells

Cases with available hematoxylin & eosin (H&E) stains were assessed for plasma cell infiltration. Plasma cells were identified by morphological features and a semiquantitative assessment was performed (0 = no plasma cells; 1 = singular plasma cells; 2 = plasma cells scattered throughout lesion or foci of 5-10 grouped plasma cells; 3 = diffuse infiltration of tumor by plasma cells or larger clusters of plasma cells (> 10 together)).

Modeling of tumor dynamics during therapy

We hypothesized that changes in tumor purity post-therapy would have the same effect on all mutations regardless of subclonal origin, while the effects of immunotherapy on mutant allele frequencies (MAFs) among non-responders would be more heterogeneous with the potential for both positive and negative selection pressures on the subclonal composition of the tumor. To evaluate this hypothesis, we modeled the change in mutant allele frequencies of single base substitutions for each patient with whole-exome sequencing data as well as both pre-treatment and on-treatment RNaseq data available. We fit a generalized linear mixed effects model with a fixed effect for the overall mean MAF pre-therapy and the overall slope describing the change in the average MAF pre- and on-therapy using the brms R package[64]. Mutation-specific MAFs pre- and on-therapy were estimated by random effects, providing some shrinkage to the overall means but with priors that were sufficiently diffuse to allow heterogeneity in the mutation-specific intercepts and slopes. The slope from this model represents the change in the tumor cell fraction between pre-treatment and on-treatment samples. To identify individual expanding or contracting mutations in a manner not explained by the general slope, we computed the probability that the slope for a mutation was different than the overall slope. Mutations with a probability of > 0.99 of being different than the overall slope were considered to be expanding if their slope was positive relative to the overall slope, and contracting if their slope was negative relative to the overall slope.

Machine learning

Integrated machine learning analysis of genomic, transcriptomic and immunologic features was performed using the randomForest and caret R packages (http://cran.r-project.org). To mitigate possible issues with feature collinearity, an approach to control inclusion of highly correlated features was applied as follows. In a given set of samples, pairwise non-parametric correlations between all possible feature pairs were calculated and these feature pairs were sorted in decreasing order of their Spearman's rank correlation coefficient. Given a maximum allowed correlation coefficient, the ordered list of feature pairs above this threshold were considered (offending pairs). Starting from the first element in the list, the feature appearing in the smallest number of other offending pairs was eliminated. If both features in the pair appeared in the same number of remaining offending pairs, these were equally likely to be eliminated and one was randomly selected. Next, any feature pair containing the eliminated feature was removed from the offending pairs list, and the process was repeated until the offending pairs list was empty. Since the final set of features included depends on the maximum allowable correlation coefficient, a sensitivity analysis to identify the optimal value of this threshold was carried out using 5 repeats of 10- fold cross-validation as follows. In each cross-validation fold, correlation coefficients were calculated using the training samples, the list of features was filtered by application of the process above for a given correlation threshold value, and the remaining features were used to train a random forest. The performance of the random forest on the test samples of the fold was recorded. The sensitivity analysis revealed that a maximum allowable value of 0.75 for pairwise feature correlation coefficients yielded the highest accuracy. Finally, pairwise feature correlations were calculated based on the entire cohort ($n = 37$, after exclusion of samples with missing feature values), the list of features were narrowed down by applying the described process using a threshold of 0.75. By doing so, we reduced the initial set of 27 features to 13 features with controlled pairwise correlations. A random forest was trained on the entire cohort ($n = 37$) using the R randomForest package. For each sample, the out-of-bag predicted probabilities were calculated; these probabilities serve as an estimate of the random forest's performance in samples not seen before. The global importance of each feature was quantified using the mean decrease in accuracy measure and was calculated as follows. The random forest was trained using all the cohort samples and the accuracy of out-of-bag predictions was recorded. Next, for each feature, the values were permuted across the dataset, and the accuracy of out-of-bag predictions was recalculated. The difference between these two accuracy estimates reflects the contribution of each feature to the classification performance. Variable importance plots displaying the relative contribution of each feature to the random forest model during cross-validation were generated using the caret package. The ROCR R package was applied for AUC evaluation of response classification accuracy based on out-of-bag predictions (http://cran.r-project.org).

QUANTIFICATION AND STATISTICAL ANALYSIS

Differences between responding and non-responding tumors were evaluated using chi-square or Fisher's exact test for categorical variables and the Mann-Whitney test for continuous variables. The Pearson correlation coefficient (R) was used to assess correlations between continuous variables and the Spearman rho coefficient was calculated for non-parametric correlations. P values were corrected using the Benjamini-Hochberg procedure and the associated false discovery rate (FDR) values were calculated.

The median point estimate and 95% CI for PFS were estimated by the Kaplan–Meier method and survival curves were compared by using the nonparametric log rank test. To evaluate statistically significant associations of genomic, transcriptomic and TCR features with PFS and OS, we performed Kaplan Meier analysis utilizing the survminer (https://github.com/kassambara/survminer) and

survival (https://github.com/therneau/survival) R packages. The log-rank test implemented in the R package coin (http://coin.r-forge.r-project.org) was applied to assess statistical significance. To optimize the final strata for each quantitative feature assessed, we evaluated a range of potential thresholds (between the 10^{th} and 90^{th} percentile across all samples) and selected the threshold that minimized the log-rank test p value.

Univariate Cox proportional hazards regression analysis was used to determine the impact of individual parameters on PFS. A multivariable Cox proportional hazards model was employed using immunoglobulin rearrangements, TCR productive clones, PD-L1 expression and expressed mutations and a risk score reflecting the relative hazard was calculated as the exponential of the sum of the product of mean-centered covariate values and their corresponding coefficient estimates for each case. The second tertile of the risk score was used to classify patients in high risk (top 33.3%) and low risk (bottom 66.6%) groups. All p values were based on two-sided testing and differences were considered significant at $p < 0.05$. Statistical analyses were done using the SPSS software program (version 25.0.0 for Windows, IBM, Armonk, NY) and R version 3.2 and higher, http://cran.r-project.org).

ADDITIONAL RESOURCES

Further information relevant to the clinical trial Checkmate 038, NCT01621490, can be found at https://clinicaltrials.gov/ct2/show/results/NCT01621490.

Cell Reports Medicine, Volume *1*

Supplemental Information

Integrative Tumor and Immune Cell Multi-omic Analyses Predict Response to Immune Checkpoint Blockade in Melanoma

Valsamo Anagnostou, Daniel C. Bruhm, Noushin Niknafs, James R. White, Xiaoshan M. Shao, John William Sidhom, Julie Stein, Hua-Ling Tsai, Hao Wang, Zineb Belcaid, Joseph Murray, Archana Balan, Leonardo Ferreira, Petra Ross-Macdonald, Megan Wind-Rotolo, Alexander S. Baras, Janis Taube, Rachel Karchin, Robert B. Scharpf, Catherine Grasso, Antoni Ribas, Drew M. Pardoll, Suzanne L. Topalian, and Victor E. Velculescu

Supplemental Information

Supplementary Figures

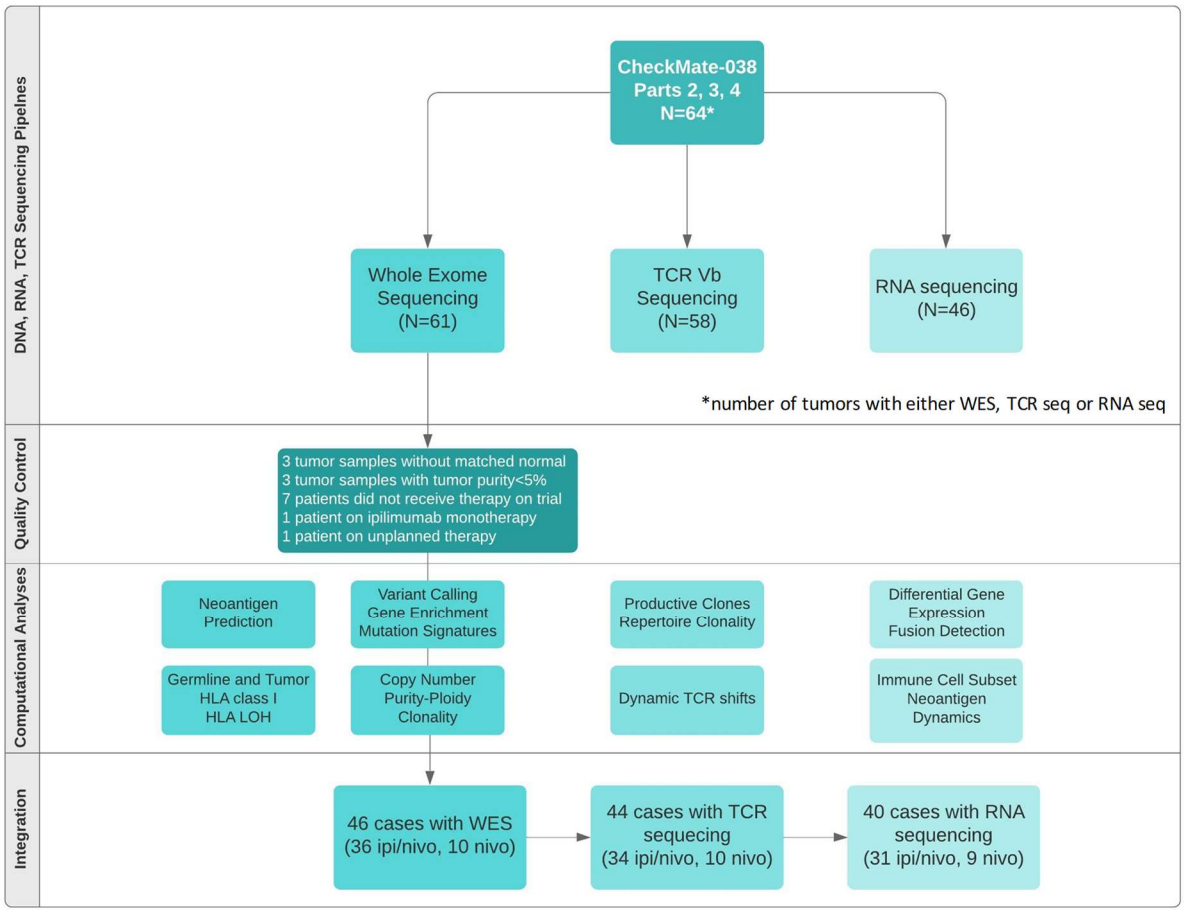

Figure S1. Overview of the whole exome, transcriptome and TCR sequencing analyses. Related to Figures 1-6. CheckMate-038 was a prospective, multi-cohort clinical trial of nivolumab as front-line therapy or after progression on therapy with ipilimumab, or receiving ipilimumab/nivolumab combination. Here, we focused on patients on parts 2, 3 and 4 which included ipilimumab-naïve patients treated either with nivolumab or combination nivolumab/ipilimumab. Sixty four tumors in parts 2, 3 and 4 had evaluable whole exome sequencing, RNA sequencing or TCR sequencing. As an initial quality control step the following cases were excluded: i. 3 tumor samples without matched normal samples, ii. 3 tumors with tumor purity less than 5%, iii. 7 patients that did not ultimately receive therapy on the CheckMate-038 trial, iv. One patient on ipilimumab monotherapy and v. One patient on unplanned therapy. Forty six baseline tumors had evaluable whole exome sequencing data which was processed for variant calling, neoantigen prediction, copy number analyses, purity-ploidy correction, HLA class I germline and somatic status assessment, gene enrichment and mutation signature analyses. Of these, forty four tumors were analyzed by TCR sequencing and forty tumors were also analyzed by RNA sequencing.

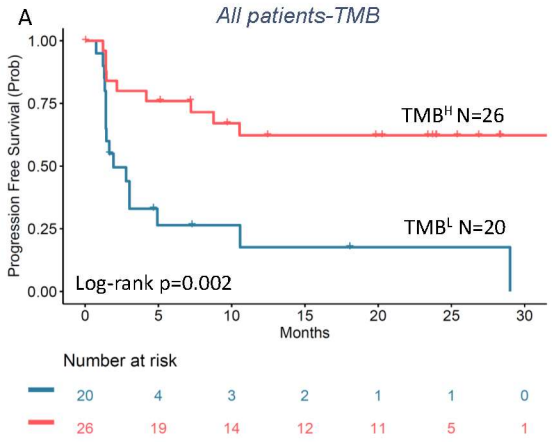
A
All patients-TMB
Progression Free Survival (Prob)
TMB^H N=26
TMB^L N=20
Log-rank p=0.002
Months
Number at risk
20 4 3 2 1 1 0
26 19 14 12 11 5 1

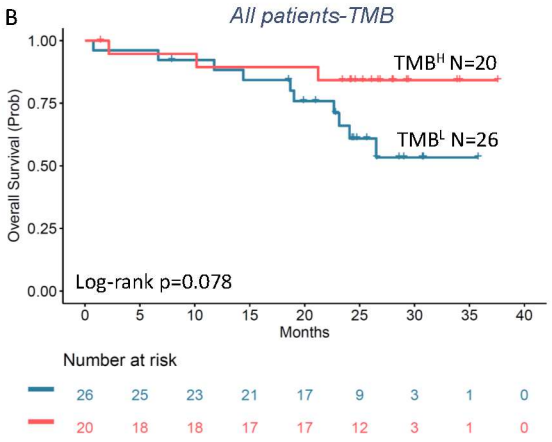
B
All patients-TMB
Overall Survival (Prob)
TMB^H N=20
TMB^L N=26
Log-rank p=0.078
Months
Number at risk
26 25 23 21 17 9 3 1 0
20 18 18 17 17 12 3 1 0

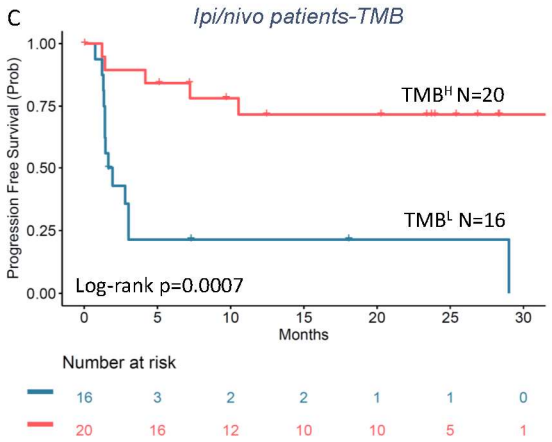
C
Ipi/nivo patients-TMB
Progression Free Survival (Prob)
TMB^H N=20
TMB^L N=16
Log-rank p=0.0007
Months
Number at risk
16 3 2 2 1 1 0
20 16 12 10 10 5 1

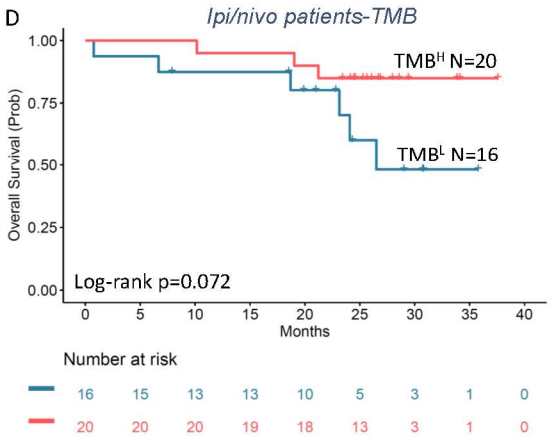
D
Ipi/nivo patients-TMB
Overall Survival (Prob)
TMB^H N=20
TMB^L N=16
Log-rank p=0.072
Months
Number at risk
16 15 13 13 10 5 3 1 0
20 20 20 19 18 13 3 1 0

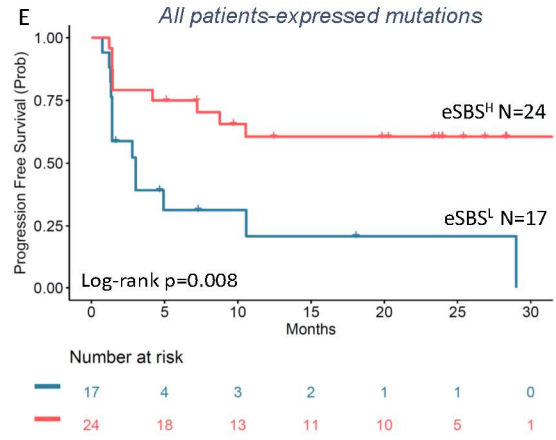
E
All patients-expressed mutations
Progression Free Survival (Prob)
eSBS^H N=24
eSBS^L N=17
Log-rank p=0.008
Months
Number at risk
17 4 3 2 1 1 0
24 18 13 11 10 5 1

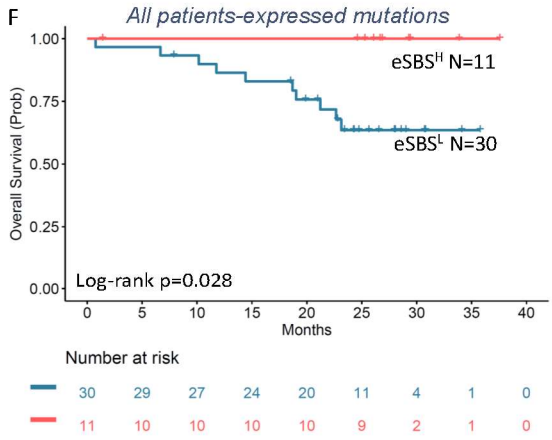
F
All patients-expressed mutations
Overall Survival (Prob)
eSBS^H N=11
eSBS^L N=30
Log-rank p=0.028
Months
Number at risk
30 29 27 24 20 11 4 1 0
11 10 10 10 10 9 2 1 0

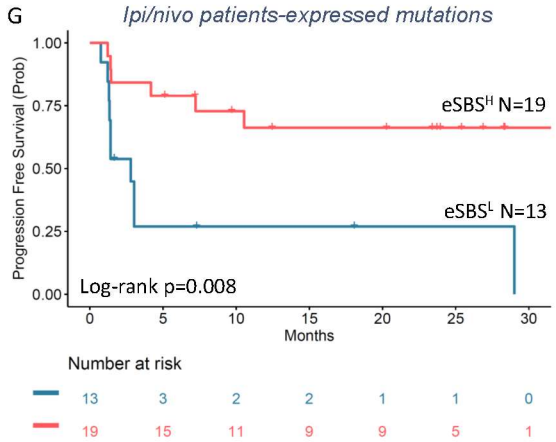
G
Ipi/nivo patients-expressed mutations
Progression Free Survival (Prob)
eSBS^H N=19
eSBS^L N=13
Log-rank p=0.008
Months
Number at risk
13 3 2 2 1 1 0
19 15 11 9 9 5 1

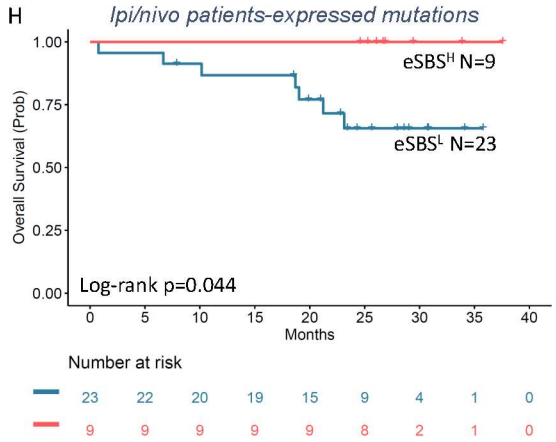
H
Ipi/nivo patients-expressed mutations
Overall Survival (Prob)
eSBS^H N=9
eSBS^L N=23
Log-rank p=0.044
Months
Number at risk
23 22 20 19 15 9 4 1 0
9 9 9 9 9 8 2 1 0

Figure S2. Association between TMB and expressed mutation load and clinical outcome. Related to Figure 1. (A) TMB predicted PFS for all patients, such that patients in the TMB-high group had a significantly longer PFS compared to the TMB-low group (median PFS not reached vs 1.938 months, HR=0.263, 95% CI: 0.114-0.609, log rank p=0.02). (B) There was a trend towards longer OS for patients with TMB-high tumors compared to the TMB-low group (median OS not reached for both groups, HR=0.334, 95% CI: 0.092-1.217, log rank p=0.078). (C) In the ipilimumab/nivolumab treatment group, high TMB conferred a favorable prognosis (median PFS for TMB-high and TMB-low patients not reached and 1.791 respectively, HR =0.171, 95% CI: 0.059-0.498, log rank p=0.0007). (D) A trend towards longer OS was observed for patients with TMB-high tumors in the ipilimumab/nivolumab treatment group (median OS not reached and 26.513 months for TMB-high and TMB-low tumors respectively, HR=0.291, 95% CI: 0.072-1.171, log rank p=0.072). (E) Single base substitutions in expressed genes were evaluated as a representation of the expressed mutation load (eSBS). Expressed mutation load predicted PFS for all patients, such that patients in the eSBS-high group had a significantly longer PFS compared to the eSBS-low group (median PFS not reached vs 3.023 months, HR=0.307, 95% CI: 0.129-0.731, log rank p=0.008). (F) Patients with eSBS-high tumors had a longer overall survival compared to the eSBS-low group (median OS not reached for both groups, log rank p=0.028). (G) In the ipilimumab/nivolumab treatment group, high eSBS conferred a favorable prognosis (median PFS for eSBS-high and eSBS-low patients not reached and 2.793 months respectively, HR =0. 245, 95% CI: 0.087-0.693, log rank p=0.008). (H) Patients with eSBS-high tumors had a longer OS compared to eSBS-low patients in the ipilimumab/nivolumab treatment group (median OS not reached for both groups, log rank p=0.044).

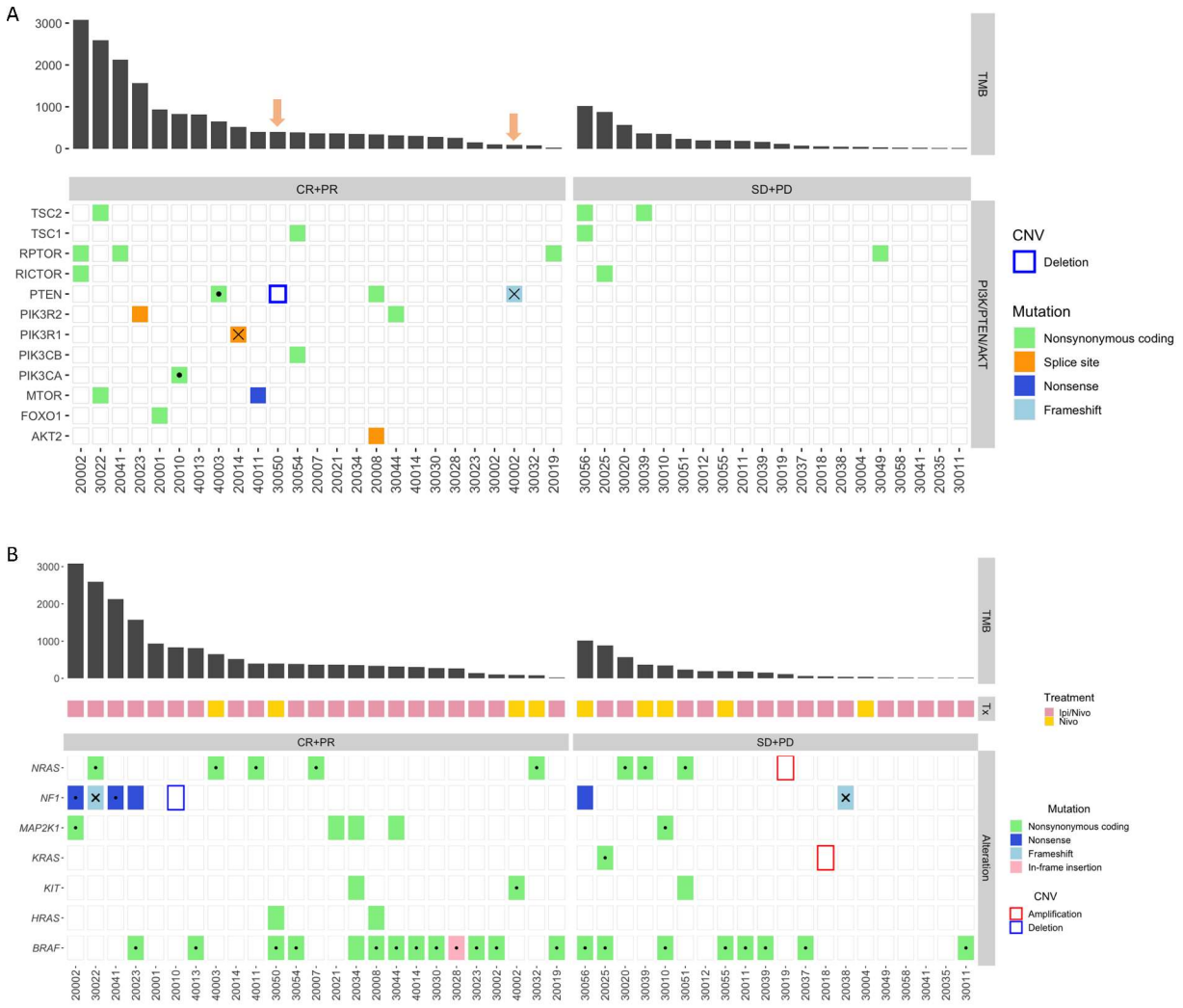

Figure S3. Differential enrichment analysis involving genes in the PI3K/AKT/PTEN and Ras pathways in tumors from responding and non-responding patients. Related to Figure 1. (A) We did not identify any significant differences in genomic alterations in the PI3K/AKT/PTEN pathway in tumors from responders vs. non-responders that could not be explained by the increased TMB of responding patients. Patient 40002, who achieved a radiographic response but had a short overall survival harbored biallelic inactivation of PTEN. In contrast, patient 30050, who achieved a long-term response to therapy, harbored a homozygous deletion in PTEN, suggesting that PTEN inactivation is not always associated with resistance to immune checkpoint blockade. We investigated co-occurrence of sequence and structural mutations in the Ras pathway and single base substitutions were characterized by consequence (missense, frameshift, nonsense, splice site, in-frame) and recurrence (hotspots). Loss of the wild type allele was considered in case of truncating mutations (biallelic inactivation, indicated as an "x"). We did not identify any significant differences in genomic alterations in the Ras pathway in tumors from responders vs non-responders that could not be explained by the increased TMB of responding patients. Dots indicate hotspot mutations.

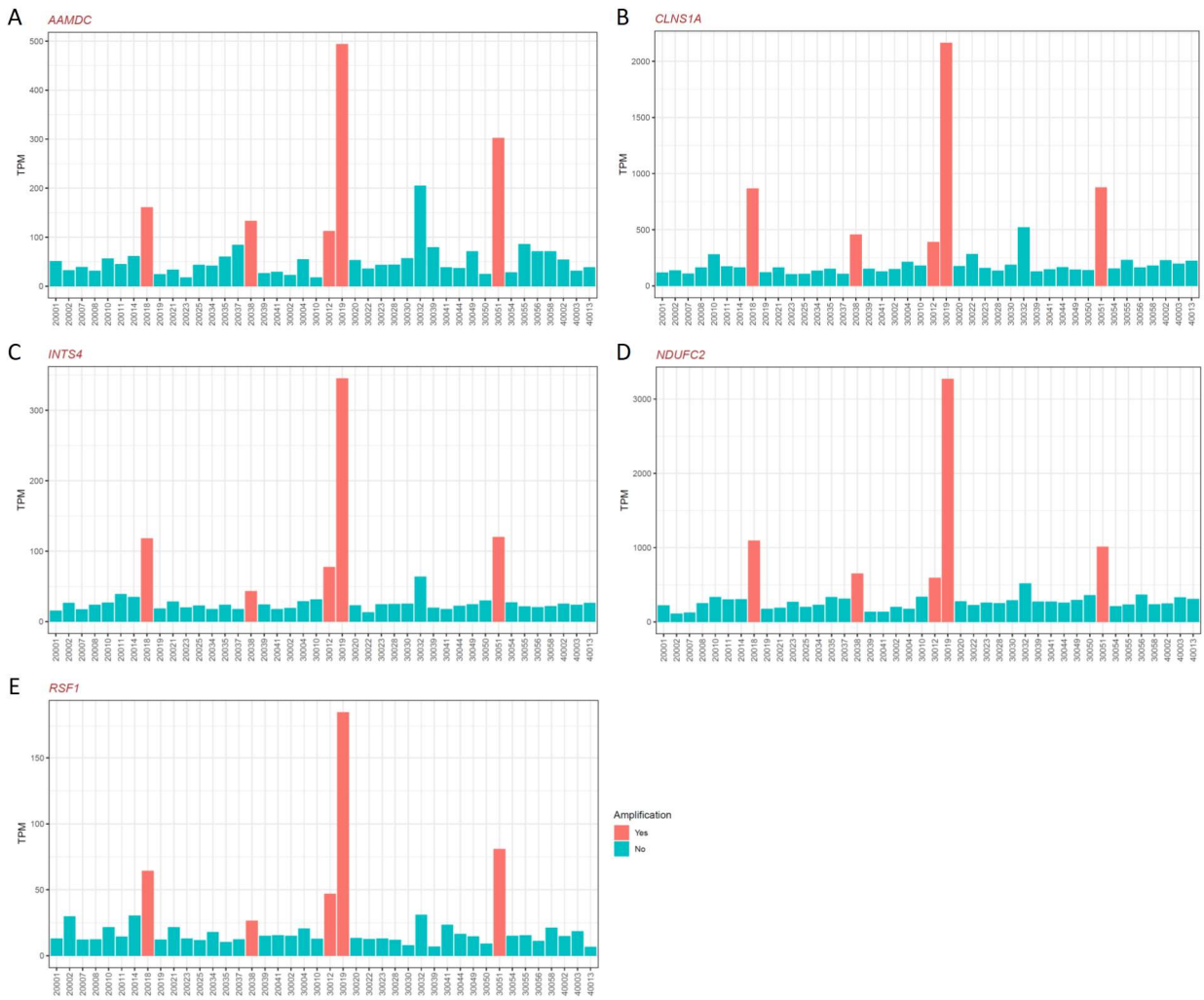

Figure S4. Gene expression of genes in the 11q14.1 locus. Related to Figure 1. Tumors from patients 20018, 20038, 30012, 30019 and 30051 that harbored an amplification in 11q14.1, we are also found to overexpress AAMDC, CLNS1A, INTS4, NDUFC2, and RSF1. Gene expression is shown in transcripts per million (TPM).

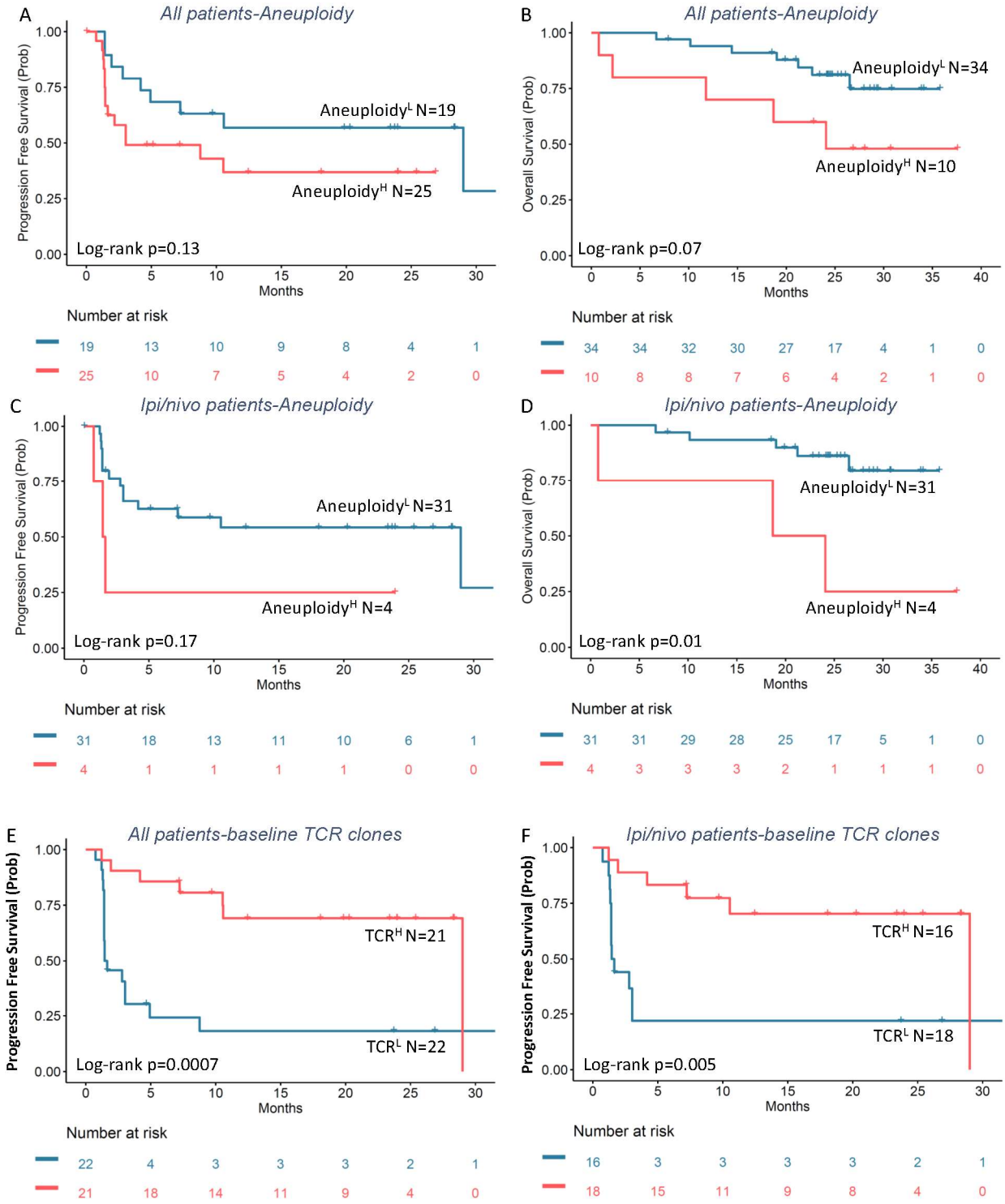

Figure S5. High tumor aneuploidy and low TCR clonotypic density identify patients with inferior outcome to immune checkpoint blockade. Related to Figures 1, 2 and 5. (A) Patients with highly aneuploidy tumors showed a trend towards shorter PFS (median PFS of 3.023 vs 29.01 for aneuploidy-high vs low tumors, HR=1.958, 95% CI: 0.818-4.689, log rank p=0.13). (B) A similar trend was observed for OS (median OS of 24.082 vs not reached for aneuploidy-high vs low tumors, HR=2.899, 95% CI: 0.919-9.152, log rank p=0.13). (C) Patients in the ipilimumab/nivolumab treatment group with highly aneuploidy tumors showed a trend towards shorter PFS (median

PFS of 1.544 vs 29.01 for aneuploidy-high vs low tumors, HR=2.749, 95% CI: 0. 0.773-9.777, log rank p=0.17). (D) Patients with highly aneuploidy tumors in the ipilimumab/nivolumab treatment group had a significantly shorter OS (median OS of 21.388 vs not reached for aneuploidy-high vs low tumors, HR=6.309, 95% CI: 1.5-26.538, log rank p=0.01). (E) An increased number of baseline intratumoral TCR productive clones predicted longer PFS for all patients (median PFS 29.01 vs 1.544 months for patients with TCR-high vs TCR-low tumors respectively, HR=0.215, 95% CI: 0.087-0.532, log rank p=0.0007) and (F) patients in the ipilimumab/nivolumab treatment group (median PFS for TCR-high and TCR-low patients 29.01 and 1.544 months respectively, HR =0.236, 95% CI: 0.086-0.649, log rank p=0.005).

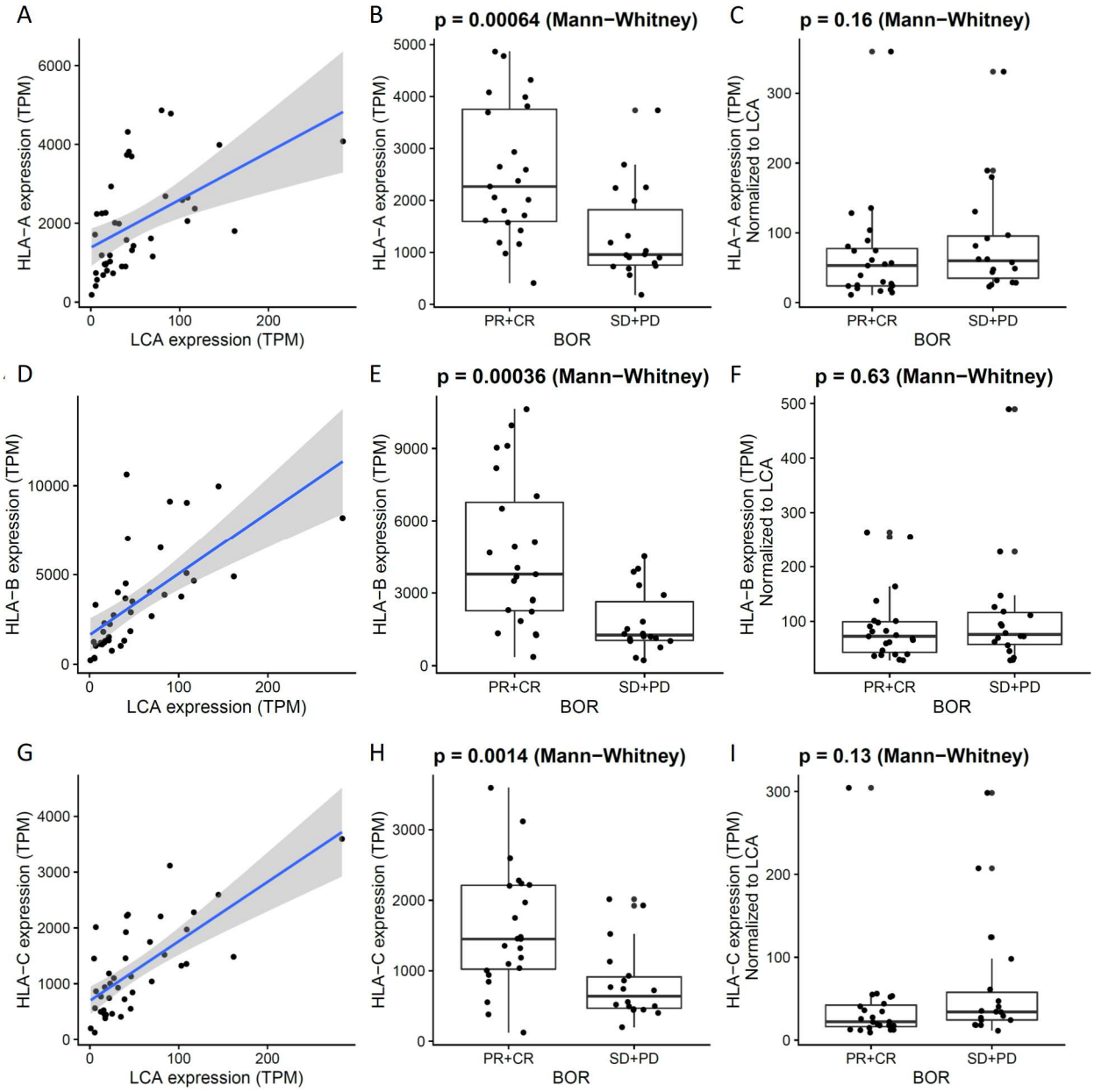

Figure S6. HLA class I genomic diversity in tumors of responding and non-responding patients. Related to Figure 2. A significantly higher expression of HLA-A (B-D), HLA-B (E-G) and HLA-C (H-J) was noted in baseline tumors from responding patients, which reflected a higher density of lymphocytic intratumoral infiltration. When HLA-A, HLA-B and HLA-C expression was normalized by LCA expression, there were no differences between tumors from responding and non-responding patients.

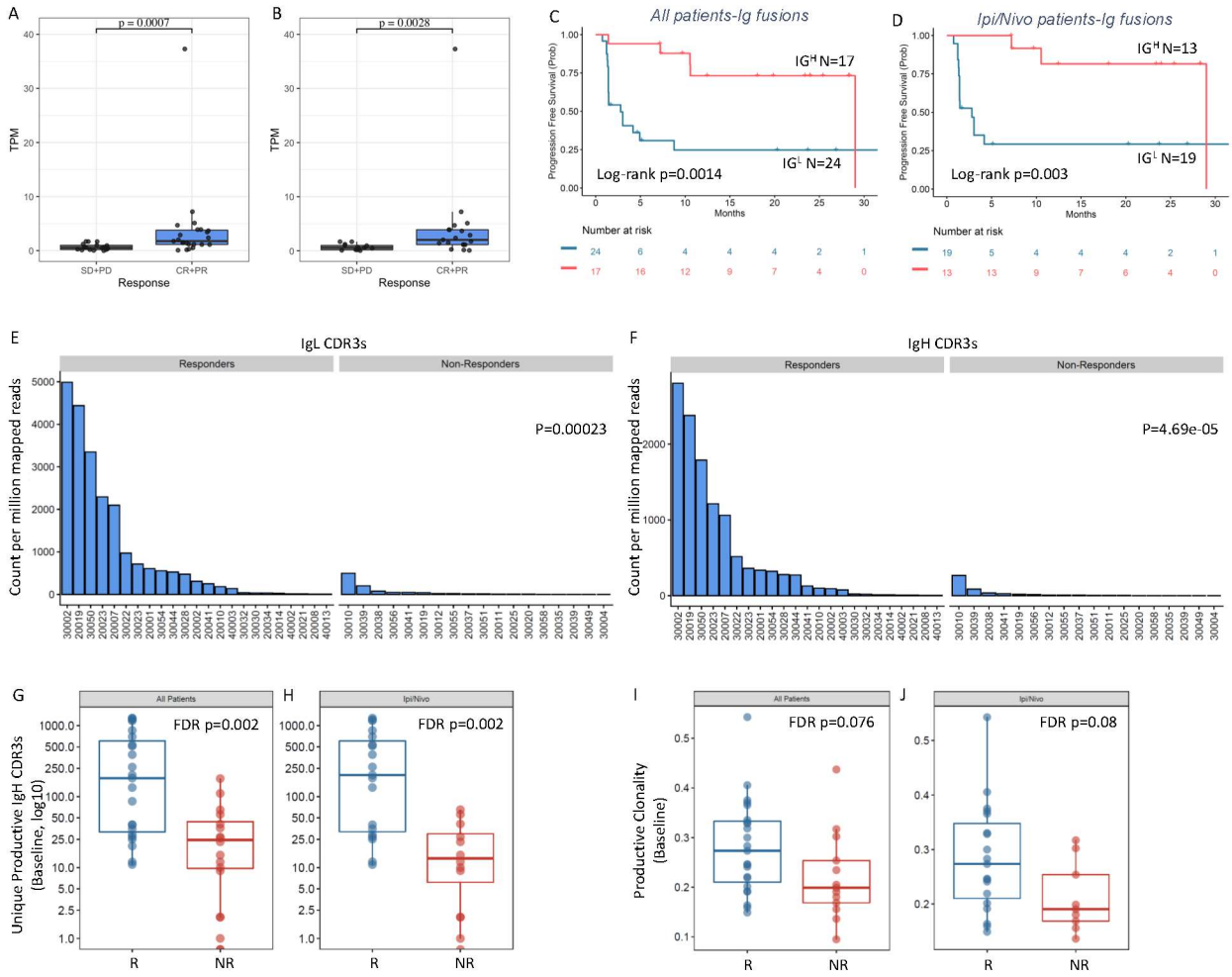

Figure S7. T and B cell features differentiate tumors from responding patients from non-responders. Related to Figures 3, 4 and 5. (A-B) Differential expression of TOX in tumors of responding and non-responding patients. A higher expression of TOX was identified in baseline tumors of responding patients (A; all patients and B; patients in the ipilimumab/nivolumab treatment group). (C-D) High number of immunoglobulin fusions is linked to a progression-free survival benefit on immune checkpoint blockade. (C) An increased number of baseline Immunoglobulin gene fusions, signifying an increased B cell density, predicted longer PFS for all patients (median PFS 29.01 vs 2.793 months for patients with Ig-high vs Ig-low tumors respectively, HR=0.217, 95% CI: 0.078,0.601, -log rank p=0.0014) and (D) patients in the ipilimumab/nivolumab treatment group (median PFS for Ig-high and Ig-low patients 29.01 and 2.793 months respectively, HR=0.180, 95% CI: 0.050-0.645, log rank p=0.003). (E-F) Differences in IgL and IgG abundance in tumors of patients with differential responses to immune checkpoint blockade. IgL and IgH chain CDR3 sequences were assembled from RNAseq data and we identified significantly higher clonal counts for both immunoglobulin light (E) and heavy (F) chains (Mann Whitney p=0.00023 and p=4.69e-05 respectively) in tumors from responding patients. (G-J) Differential IgH CDR3 abundance analysis in baseline tumors. (G-H) A higher IgH CDR3 clonal count was noted in tumors from responding patients for all patients (FDR adjusted p=0.002) and patients in the ipilimumab/nivolumab treatment group (FDR adjusted p=0.002). (I-J) A trend towards a more clonal BCR repertoire was observed for all patients (FDR adjusted p=0.076) and patients in the ipilimumab/nivolumab group (FDR adjusted p=0.08). TPM; transcripts per million.

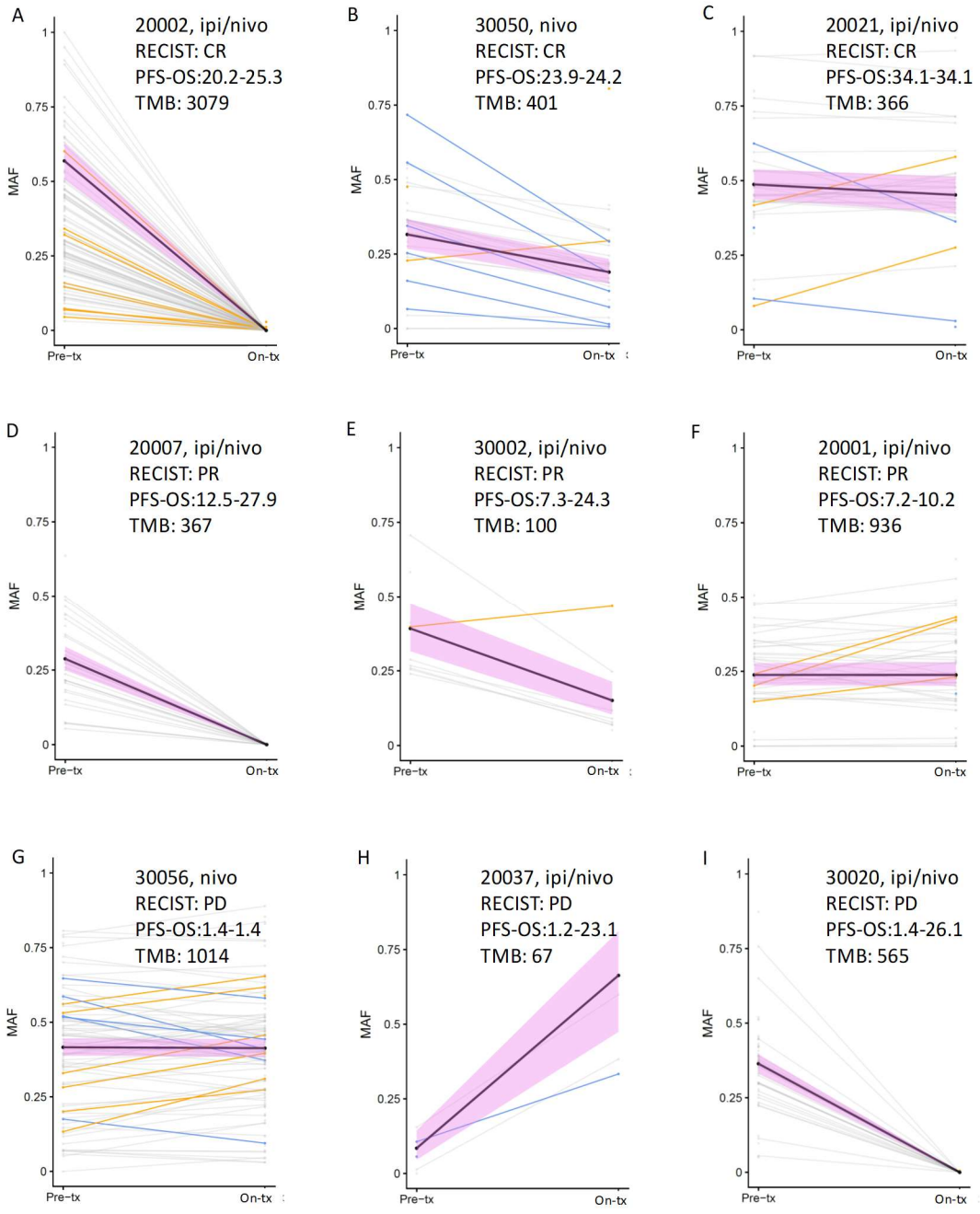

Figure S8. Expressed mutation dynamics during immune checkpoint blockade. Related to Figure 1. A Bayesian generalized linear multilevel mixed-effects model was implemented to interpret changes in mutant transcript levels between pre-treatment and on-treatment tumors. We fit a generalized linear mixed effects model with a fixed effect for the overall mean mutant allele fraction (MAF) pre-therapy and the overall slope describing the change in the average MAF pre- and on-therapy (dark black line with 95% confidence band shaded in purple). Mutations covered by at least 75 reads at both time points are shown and are colored orange if there is >0.99 probability that their slope is positive relative to the overall slope, and blue is there is a >0.99 probability that their slope is negative relative to the overall slope. Panels A, D, E and I correspond to molecular responders with MAFs that uniformly decreased to undetectable levels post-therapy and molecular responses reflected clinical outcomes. Patient 30020 (I) showed a clear pattern of molecular response that was reflected in a long overall survival of 26.1 months, but not captured by early radiographic assessments which showed disease progression at 1.4 months. Responding patient 20021 (C) showed a pattern of expressed mutation retention, most likely due to timing of tumor

biopsy that may have preceded tumor clearance. Panels F, G and H show molecular non-responders, denoted as retention of expressed mutations, with evidence of both positive- and negative- selective pressures of therapy (orange and blue lines respectively) that cannot be explained by overall difference in mean MAFs (black line). Patient 20001 (F) showed a molecular progression pattern that was reflective of a short OS of 10.2 months, despite a radiographic response assessment of partial response.

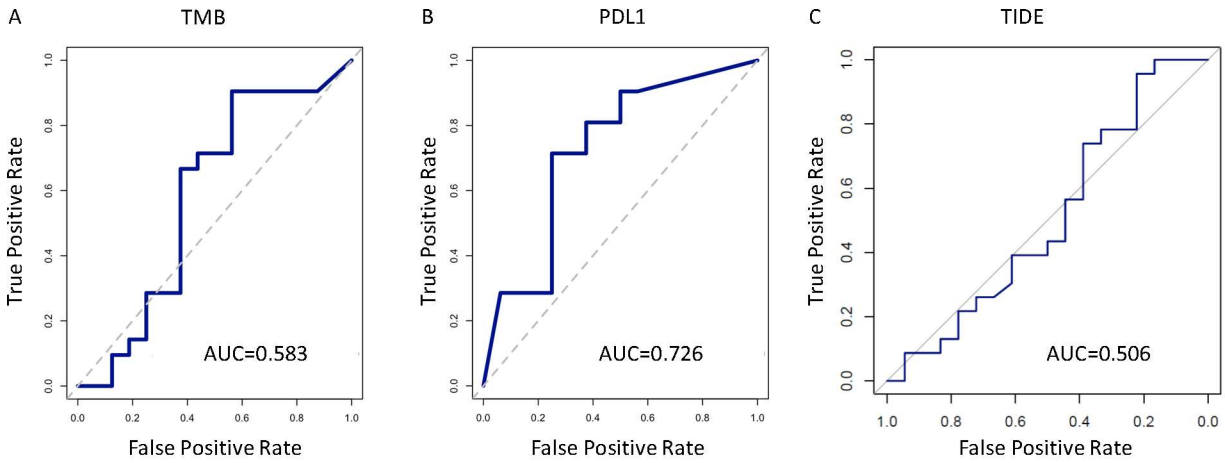

Figure S9. Predictive accuracy of TMB and PD-L1 expression. Related to Figure 6. (A) TMB and (B) PD-L1 expression demonstrated a moderate prediction accuracy with an AUC of 0.583 (95% CI: 0.377-0.79) and 0.726 (95% CI: 0.552-0.9) respectively. (C) The TIDE algorithm was not predictive of outcome in this cohort (AUC=0.506).